Enhancing Capacitance Performance of $Ti_3C_2T_x$ MXene as Electrode Materials of Supercapacitor: From Controlled Preparation to Composite Structure Construction

Xiaobei Zang[1], Jiali Wang[1], Yijiang Qin[1], Teng Wang[1], Chengpeng He[1], Qingguo Shao[1], Hongwei Zhu[2], Ning Cao[1] ✉

✉ Ning Cao, caoning1982@gmail.com

[1] School of Materials Science and Engineering, China University of Petroleum (East China), Qingdao 266580, People's Republic of China

[2] School of Materials Science and Engineering, Tsinghua University, Beijing 100084, People's Republic of China

HIGHLIGHTS

- The traditional and novel etching methods are summarized and compared, especially fluorine-free method. The methods for accelerating exfoliation of $Ti_3C_2T_x$ are classified.

- The energy storage mechanisms of $Ti_3C_2T_x$ in different electrolytes are compared. Based on energy storage mechanisms, the influencing factors of morphology and surface functional groups are discussed.

- In response to the problems of the $Ti_3C_2T_x$, strategies for improving capacitance from structure modulation to composite structure construction are summarized and compared.

ABSTRACT $Ti_3C_2T_x$, a novel two-dimensional layer material, is widely used as electrode materials of supercapacitor due to its good metal conductivity, redox reaction active surface, and so on. However, there are many challenges to be addressed which impede $Ti_3C_2T_x$ obtaining the ideal specific capacitance, such as restacking, re-crushing, and oxidation of titanium. Recently, many advances have been proposed to enhance capacitance performance of $Ti_3C_2T_x$. In this review, recent strategies for improving specific capacitance are summarized and compared, for example, film formation, surface modification, and composite method. Furthermore, in order to comprehend the mechanism of those efforts, this review analyzes the energy storage performance in different electrolytes and influencing factors. This review is expected to predict redouble research direction of $Ti_3C_2T_x$ materials in supercapacitors.
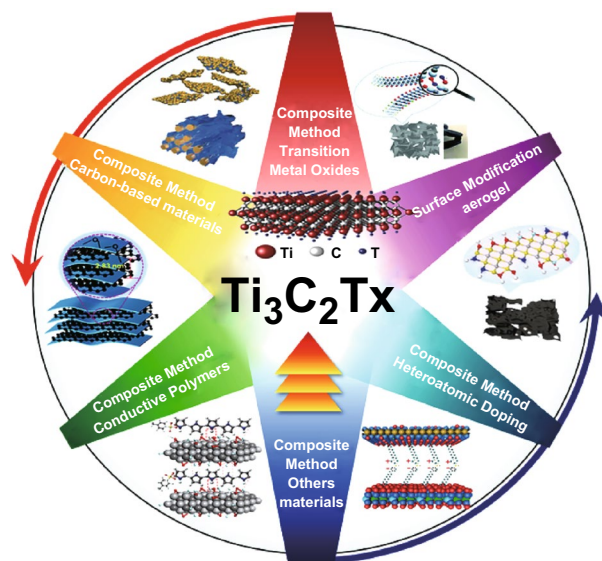
1 Introduction

With the deterioration of environment and the depletion of traditional fossil energy, renewable and sustainable energy has been attracted much attention [1, 2]. However, the supply of these kinds of energy is intermittent, due to their dependence on weather. As supplementary, energy storage devices have drawn tremendous interest recently [3, 4]. Supercapacitors, one of new energy storage devices between batteries and traditional parallel-plate capacitors, have the characteristic of high power density, rapid charge/discharge rate, and excellent cycle stability [5, 6]. Electrode materials are one of the critical factors affecting the capacitance performance of supercapacitors. The common electrode materials include carbon-based materials [7–9], transition metal oxides (TMOs) [10], conductive polymers (CPs), and so on [11–14]. Nevertheless, the prior researches have proved that the low density of carbon-based materials, the poor conductivity of TMOs, and the instable structure of CPs hinder them from achieving ideal capacitance performance [15, 16]. Therefore, there is still a significant challenge to improve the performance of electrode materials of supercapacitors for practical use.

In 2011, an interesting two-dimensional material named MXene was synthesized by Gogosti [17]. MXene is a novel two-dimensional (2D) layered material composed of transition metal carbides and/or nitrides, and it is formed through selectively etching the A layers from MAX precursor, where M represents transition metals, such as Ti, Zr, Nb, Ta, and Mo and X represents carbon and/or nitrogen [18–21]. Many MXene materials have been studied recently, such as $V_2C_2T_x$, $Ti_3C_2T_x$, and Ti_2CT_x. [22, 23]. In the formula, T_x is the surface functional group introduced by etching condition, such as –O, –F, and –OH [24, 25]. Due to its low formation energy, $Ti_3C_2T_x$ is the first and one of the most widely studied MXene materials [26]. $Ti_3C_2T_x$ overcomes the shortcomings in general electrode materials, and it has become a hot spot in supercapacitors. Even so, there are still many problems to be solved, as follows: (1) $Ti_3C_2T_x$ has ultrahigh volume specific capacitance ascribed to its high density (~ 3.8 g cm^{-3} in $Ti_3C_2T_x$ film) [27]. However, the self-restacking caused by the van der Waals force restricts active surface utilization. Besides the irreversible stacking between $Ti_3C_2T_x$ layers, the aggregation resulting from the effect of hydrogen bonding also restrains the redox reaction
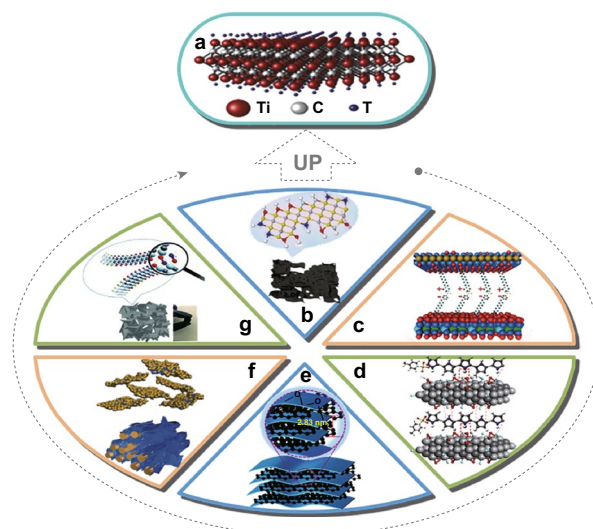

Fig. 1 Enhancing the capacitance of $Ti_3C_2T_x$ as electrode materials of supercapacitors. **a** Structure of $Ti_3C_2T_x$ [21]. **b** N-doped $Ti_3C_2T_x$ [36]. **c** $Ti_3C_2T_x$/layered metallic double hydroxides [37]. **d** $Ti_3C_2T_x$/conductive polymers [41]. **e** Carbon-intercalated $Ti_3C_2T_x$ composite paper [38]. **f** $WO_3/Ti_3C_2T_x$ composite paper [39]. **g** 3D $Ti_3C_2T_x$ aerogels [40]. Reproduced with permission from Refs. [21, 36–40]

of $Ti_3C_2T_x$ edges [28, 29]; (2) structure stability is a critical factor influencing the cycle performance. During the charge and discharge, it is unavoidable to incur the volume change, leading to large structural stress. If the stress exceeds the strength of $Ti_3C_2T_x$, it is clear that structural deformation and damage will happen, which are manifested by the lamellar re-crushing or shedding of active materials from electrode [30]; (3) the adsorption of oxygen or water molecules may partially oxidize $Ti_3C_2T_x$ to non-conductive titanium dioxide (TiO_2), which will reduce redox reaction active sites and increase the charge transfer impendence [30, 31]. This defect is particularly significant in the hydrothermal method [32].

In order to control those situations, many works have focused on the modification of $Ti_3C_2T_x$ [33–35]. Figure 1 shows the common methods of enhancing the capacitance of $Ti_3C_2T_x$ as electrode materials of supercapacitors [21, 36–41]. With the efforts of predecessors, many interesting ideas about enhancing capacitance have been put forward, such as modification of preparation process, surface modification, and composite methods. The self-stacking obstacle can endure by increasing the layer space, pillaring effect, and other measurements. In addition, one of the strategies for maintaining structural stability is to increase

the strength of the materials. Wang et al. [16] prepare a vacuum-filtered $Ti_3C_2T_x$/PDA film after dopamine self-polymerized on the $Ti_3C_2T_x$ nanosheets into the layered polydopamine (PDA). The interlayer of PDA increases the layer space of $Ti_3C_2T_x$ solving the self-stacking during cycling. Dopamine forms hydrogen bonding with surface functional groups, while Ti forms strong bonding with oxygen atoms in polydopamine, which help strengthen the materials and maintain the stability of the structure [16]. Naguib et al. [42] mixed the $Ti_3C_2T_x$ with polyacrylamide (PAM) and dried it into composite film, where the $Ti_3C_2T_x$ nanoflakes are dispersed in a network formed by PAM. Placing $Ti_3C_2T_x$ in the 3D network also helps maintain structural stability. The oxidation of $Ti_3C_2T_x$ is avoided through controlling the temperature and using reducing atmosphere in the laboratory [43, 44].

In this review, we devote to the brief summarization of the approaches for improving the electrochemical property of $Ti_3C_2T_x$ as the electrode materials of supercapacitors, including the preparation process, surface terminations, precursor, electrolyte, and other governing factors. We hope that it will provide the guidance for further research of $Ti_3C_2T_x$ in supercapacitors.

2 Properties of $Ti_3C_2T_x$

As the representative candidate of electrode materials, $Ti_3C_2T_x$ owns the 2D structure like famous materials—graphene. The atomic composition model is shown in Fig. 2a [25]. In contrast to carbon materials, $Ti_3C_2T_x$ contains metal element contributing to high density and surface functional group simultaneously. On account of its special composition, $Ti_3C_2T_x$ is provided with unique characteristics. Owing to the high density of $Ti_3C_2T_x$ compared with carbon-based materials, its volumetric capacitance is higher. $Ti_3C_2T_x$ has metal conductivity combined with hydrophilicity which guarantees the fast electron transfer and wetting of electrolyte. The adjustable surface functional groups T_x lead to a change in outward structure to meet different needs. T_x, particularly –O, on the surface of $Ti_3C_2T_x$ provide many active sites for redox reaction [45]. Furthermore, the surface is negatively charge due to the negative surface functional groups, and it behaves hydrophilicity through hydrogen bonding between water and T_x, contributing to the good dispersibility in aqueous solution [29, 46]. Normally, the oxidation of $Ti_3C_2T_x$ is controlled by external temperature. Therefore, it is of great significance to study its thermal stability. When

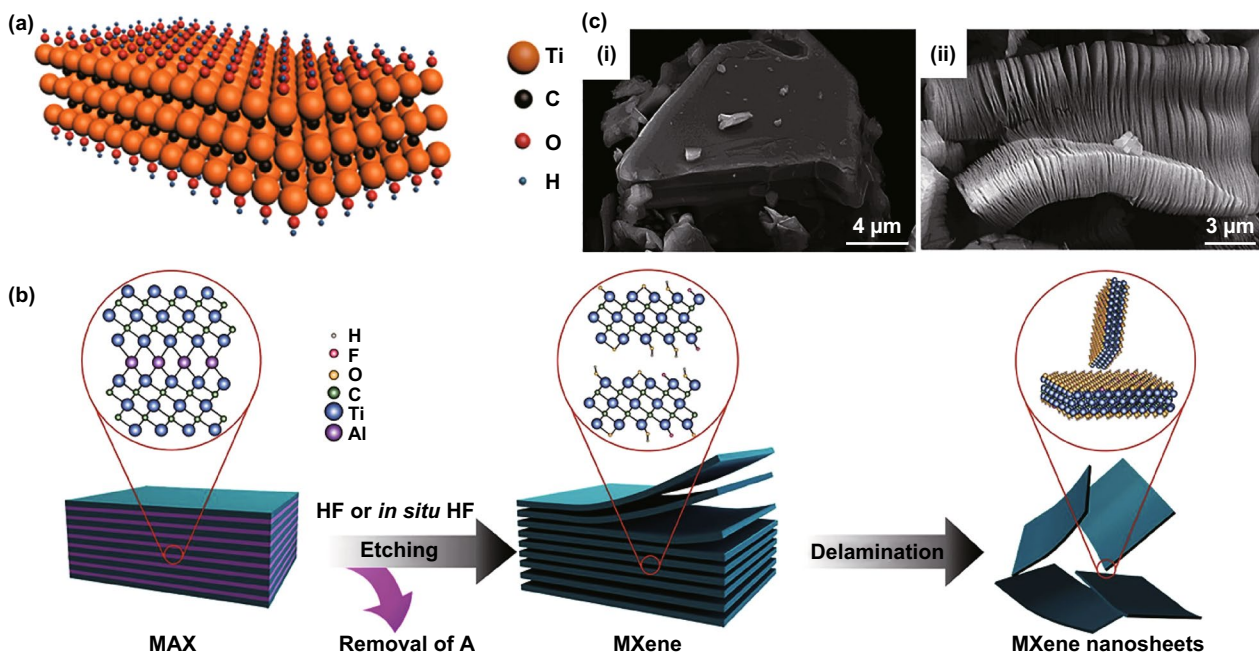**Fig. 2** Structure of $Ti_3C_2T_x$. **a** Atomic composition model of $Ti_3C_2T_x$ [25]. **b** Schematic diagram of the process for etching and delamination of Mxene [51]. **c** Scanning electron microscopy (SEM) images of Ti_3AlC_2 particle and $Ti_3C_2T_x$ [23]. Reproduced with permission from Refs. [23, 25, 51]

$Ti_3C_2T_x$ is heated, the changes are completed in four stages. As the temperature increases, interlayer water (100 °C), –OH (200–400 °C), and –F (500–800 °C) are gradually removed, eventually resulting in the carbonization of $Ti_3C_2T_x$ [47].

Stemming from its unique structure and properties, $Ti_3C_2T_x$ has been considered the candidate to amend imperfections of common electrode materials of energy storage, except to water purification [48, 49], photo-electrocatalyst, and electromagnetic shielding [50, 51]. $Ti_3C_2T_x$ can be used as reinforcement to improve electrochemical properties of other materials, such as CPs and TMOs [42, 52]. Zhu et al. utilized electrophoretic deposition intercalated polypyrrole (PPy) in $Ti_3C_2T_x$, forming interconnected structure [41]. The stabilized layered structure of $Ti_3C_2T_x$ improves the structural stability of PPy composites impeding the volume contraction/expansion during cycling. Moreover, $Ti_3C_2T_x$ as a substrate for growth of MnO_2 particles ensures its uniform distribution and the good metal conductivity of $Ti_3C_2T_x$ to provide the conditions for rapid electron transport of the hybrid films [53].

3 Preparation of $Ti_3C_2T_x$

There are two strategies to synthesize 2D $Ti_3C_2T_x$: top-down and bottom-up methods. In this review, we discuss some common top-down methods, such as HF-etching, LiF–HCl etching, and fluoride-free etching. Generally, the synthesis of $Ti_3C_2T_x$ includes four main steps, as shown in Fig. 2b [51]: preparation of Ti_3AlC_2 (Fig. 2c(i)) [23], etching Al layer, intercalation, and exfoliation. The common etching measurements are implemented by HF-etching and LiF–HCl etching, as showing in Eq. 1 [17, 54]. Then, the surface of 2D Ti_3C_2 is covered by –O, –OH, and –F forming $Ti_3C_2T_x$.

$$Ti_3AlC_2 + 3H^+ + 3F^- = AlF_3 + 3/2H_2 + Ti_3C_2 \qquad (1)$$
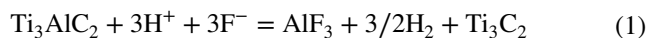
The main difference between the two methods is that the latter one has lithium ion intercalation during etching, which both increases the distance between $Ti_3C_2T_x$ layers, the area of $Ti_3C_2T_x$ flakes, and the number of hydroxyl functional groups. HF-etching requires the cation intercalation to assist in delaminating $Ti_3C_2T_x$ into single or few layer sheets, and the morphology of HF–$Ti_3C_2T_x$ is shown in Fig. 2c(ii) [23]. And HF–$Ti_3C_2T_x$ has small hole defects that makes active titanium ion expose to the air and aggravates the oxidation process, forming TiO_2. LiF–HCl etching method

is also called the clay method, because of clay-like behavior of LiF–HCl–$Ti_3C_2T_x$. LiF–HCl–$Ti_3C_2T_x$ is hydrophilic owing to abundant –OH. In the etching process, the volume expanses almost twice, as a consequence of the hydration of intercalated lithium [55]. The extent of volume expansion depends on the hydration enthalpy or hydration radius of the cation. Besides, the etching trace is in positive correlation with the content of LiF and HCl, where lithium ion intercalation depends on the former, while the degree of reaction depends on the latter. Compared with the HF-etching method, the LiF–HCl etching method is milder and the etching product has higher surface quality and better mechanical stability, since the size of the nanosheet is larger without ultrasonic treatment in the exfoliating process.

In addition, the morphology of $Ti_3C_2T_x$ is affected by the etching temperature, etching time, ball milling time of precursors in both etching methods. For example, surface functional groups introduced by etching inhibit further etching of Al layer; the increasing etching temperature accelerates the etching rate and degree [56]; the conductivity is better when the ball milling time is longer, which causes the greater destroy of interlayer van der Waals force and the more exposure of the carbon ions [57]. However, when the etching time is too long, $Ti_3C_2T_x$ sheets will be corroded into holes or even damaged for the corrosion of titanium atoms [58].

There are the other etching methods to obtain $Ti_3C_2T_x$ sheets. Many studies focus on avoiding the use of fluorine-containing reagents. Yang et al. [59] prepared $Ti_3C_2T_x$ by an electrochemical etching method, using ammonium chloride (NH_4Cl) as the electrolyte and Ti_3AlC_2 as the anode in a particular voltage range. Since the intensity of Al–Cl bond is stronger than that of the Al–Ti, the Al can be etched by Cl^- to form Al–Cl. Furthermore, the open structure is formed by ammonium ions intercalated uniformly. The increase in layer space avails the permeation of Cl^-, accelerating the etching process. Specially, the structure of $Ti_3C_2T_x$ in this study is dense instead of the common accordion shape, because less gas is released during etching. Li et al. successfully build the 2D $Ti_3C_2T_x$ nanosheets by KOH-etching [60]. In this method, KOH mixed with small amounts water reacts with Al layers releasing H_2. Meanwhile, the extraction of Al layer leads to the adhering of –OH during the etching and exfoliation process. The merits of those fluoride-free etching process compared with the traditional methods (HF-etching and LiF–HCl etching) include

operational performance and capacitance performance of $Ti_3C_2T_x$. As we all know, HF is one of the most dangerous reagents in the laboratory. As a result, one of the advantages of this fluoride-free process is to avoid the safety hazards of using HF-etching or in-situ HF-etching; the other is that the prepared $Ti_3C_2T_x$ does not contain –F, which harms the specific capacitance. The effects of –F are discussed later in detail. Interestingly, the main purpose of etching is to remove the Al layer while maintaining the original layered structure. But some researches indicate the appropriate residue of Al will improve the conductivity of $Ti_3C_2T_x$. Guo et al. [30] found that a part of Al layers is retained using hydrothermal method with the intercalation of potassium ions. It is beneficial for $Ti_3C_2T_x$ to maintain a stable layered structure. The retained Al elements form electron transfer channels to improve conductivity. Meanwhile, the space left by removing Al elements is favorable for the penetration of electrolyte ions in supercapacitors.

The exfoliation is a necessary process for obtaining single layer or few layers of $Ti_3C_2T_x$. At present, there are many methods for accelerating the exfoliation of materials, including: (1) mechanical methods: Feng et al. [56] showed the ultrasonic treatment-assisted exfoliating process could inhibit the formation of a stable force between layers to obtain $Ti_3C_2T_x$ sheets with rich functional groups on the surface, but also cause the problem of a small lateral dimension. (2) The introduction of repulsion groups: Qian et al. [61] revealed that the repulsion between the methyl group of dimethyl sulfoxide (DMSO) organic intercalant and the hydroxyl group on the surface of $Ti_3C_2T_x$ contributes to increase the interlayer spacing. Meanwhile, –F is replaced partly by a hydroxyl group during the exfoliating, leaving the high boiling organic reagent [62]. As a result, it is difficult to remove impurities. (3) The hydrothermal method: It is well known that the increase in the temperature of solvent can heighten the energy of the intercalated ions, which accelerates the diffusion of the intercalation reagent to break the energy barrier of the Ti–Ti bond, but the oxidation phenomenon of $Ti_3C_2T_x$ tends to increase during the hydrothermal reaction [63]. It is necessary to add antioxidant for inhibiting the process. (4) The ion-assisted intercalation: The TMAOH polar molecules are candidates for intercalation materials, because it is easy to enter the interlayer van de Waals force and react with the remaining Al. The formed aluminum hydroxide can further increase the interlayer spacing. Ion-assisted intercalation, an important exfoliating method,

mainly depends on the diameter of the ions and the relative size of the layer spacing. That is the reason why the intercalation efficiency of Li ions is significantly higher than that of other metal cations, as shown in Fig. 3a [64]. It should be noted that the material avoids attaching at the edge of $Ti_3C_2T_x$ as a consequence of large diameters.

4 Capacitance Properties

According to the energy storage mechanism, the supercapacitor can be divided into two categories: (1) electric double-layer capacitor, in which ions are adsorbed by an electrical layer between the electrolyte and the electrode [65, 66]; (2) pseudocapacitance, which utilizes a rapid Faradic reaction occurring on the surface of the electrode to store energy [67].

With regard to $Ti_3C_2T_x$, it exhibits different capacitance characteristics, which depends on the size of electrolyte cations, the functional groups, the status of interlayer water, the morphological structure, and so on. In particular, the $Ti_3C_2T_x$ nanosheet is negatively charged with negative functional groups like –F, –O, and –OH. When electrolyte cations move in $Ti_3C_2T_x$ layers, it produces the electrostatic attraction between opposite charges. At this time, if the electrolyte cation is small enough to pass through $Ti_3C_2T_x$ layers, which causes the electrode to be deformed, additional pseudocapacitance is generated. Conversely, the larger ions cannot penetrate into layers and can only form electrostatic repulsion at the edge of the intercalation layer to maintain high cycle stability, and the electric double-layer capacitance is formed by electrochemical adsorption.

4.1 Electric Double-Layer Capacitance

Electric double-layer capacitor is similar to traditional parallel capacitor in that it forms an electrical layer between the electrode and electrolyte to store energy, where the polar solvent between the electrode and ions serves as the electrolyte [68, 69]. This formation characteristic determines that the specific surface area of the electrode material affects the amount of ions absorbed. If the surface area increases or the distance of ions diffusion reduces, the specific capacitance of $Ti_3C_2T_x$ may be enhanced. This may provide a new opinion for enhancing the capacitance of $Ti_3C_2T_x$ in further research. In neutral aqueous electrolyte or organic electrolyte, the

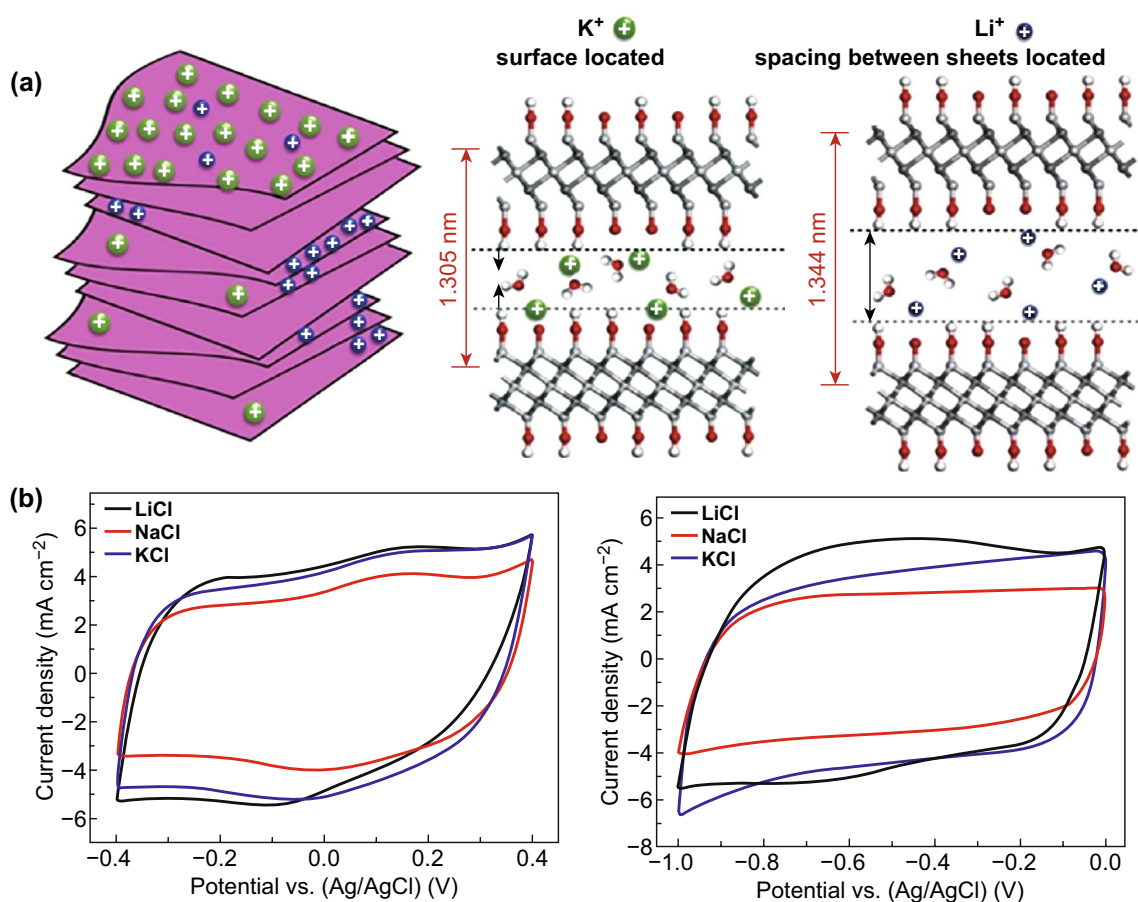**Fig. 3** Electrochemical performance of $Ti_3C_2T_x$ at a scan rate of 5 mV s^{-1}. **a** Schematic illustration of ionic intercalation mechanism on the surface of the $Ti_3C_2T_x$. **b** CV curves of $Ti_3C_2T_x$ in aqueous LiCl, NaCl, and KCl electrolyte at different potential windows. Reproduced with permission from Ref. [64]

energy storage mechanism of $Ti_3C_2T_x$ may behave as electric double-layer capacitance [27, 64]. Moreover, whether electric double-layer capacitance can be formed in the $Ti_3C_2T_x$ depends on the diameter of electrolyte ions and the relative size of interlayer spacing. If the diameter of electrolyte ions is smaller than the layer space, the energy is stored by intercalation instead of electroadsorption. Qian et al. study the change of capacitance associated with cation [60]. As shown in Fig. 3b, the CV curves of electric double-layer capacitance are typical rectangular profiles without redox peak [64] and there is no obvious voltage drop in the beginning of the charge and discharge. At the same time, the specific capacitance contributed to electric double-layer capacitance is mainly controlled by ionic concentration. Xia et al. using a simulated seawater solution (0.6 M NaCl) measured $Ti_3C_2T_x$ which has specific capacitance of only 67.7 F g^{-1} (1 A g^{-1}) [70]. Although this type of electrolyte is low in cost and high

in safety, we can infer from the capacitance performance that a small number of ions leads to low ion conductivity and a few adsorbed ions. Compared with pseudocapacitance, this energy storage mechanism is not extensive, so there are few related investigations.

4.2 Pseudocapacitance

4.2.1 The Influence of Electrolyte

4.2.1.1 Aqueous Electrolyte One of the most common aqueous electrolytes is sulfuric acid electrolyte. Since the cation in the sulfuric acid electrolyte is a small-sized hydrogen ion, it is permeable to the nanosheet layer and causes high ionic conductivity. When $Ti_3C_2T_x$ is in the sulfuric acid electrolyte, the storage mechanism of pseudocapacitance is dominant [71, 72]. The intercalation of hydrogen ions pro-
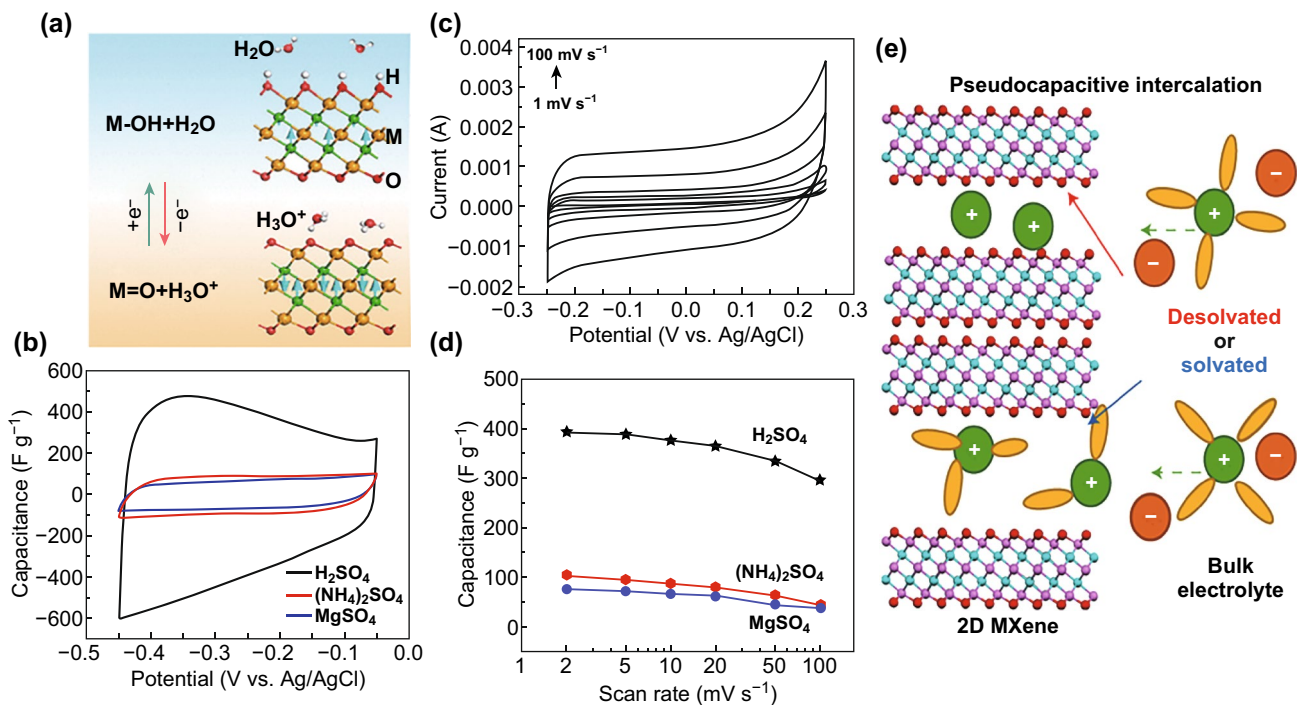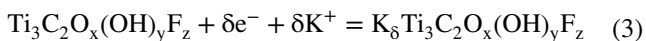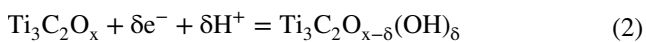
Fig. 4 Pseudocapacitance of $Ti_3C_2T_x$ in different electrolytes. **a** The change of surface group of $Ti_3C_2T_x$ in H_2SO_4 [58]. **b** CV curves of $Ti_3C_2T_x$ at a scan rate of 20 mV s^{-1} [71]. **c** Gravimetric capacitances of $Ti_3C_2T_x$ at different scan rates [75]. **d** CV curves of $Ti_3C_2T_x$ at different scan rates in KOH electrolyte [75]. **e** Schematic of supercapacitor using $Ti_3C_2T_x$ (pink, Ti; cyan, C; red, O) as negative electrode with solvated or desolvated states. Legend for the electrolyte: green, cation; orange, anion; yellow, solvent molecule [81]. Reproduced with permission from Refs. [58, 71, 75, 81]. (Color figure online)

tonates the oxygen functional group on the surface, forming a hydroxyl group (Fig. 4a, b) [58, 71], and the oxidation state of Ti is changed. The reversible change of the Ti oxidation valence state from +3 to +4 follows bonding and bond-breaking of the oxygen functional group, respectively [73]. Briefly, the above electrochemical reaction can be described by Eqs. 2 and 3:

$$Ti_3C_2O_x + \delta e^- + \delta H^+ = Ti_3C_2O_{x-\delta}(OH)_\delta \qquad (2)$$

$$Ti_3C_2O_x(OH)_yF_z + \delta e^- + \delta K^+ = K_\delta Ti_3C_2O_x(OH)_yF_z \quad (3)$$

It can be seen from Eq. 2 that the increasing concentration of sulfuric acid further improves the ion conductivity of the electrolyte to enhance the specific capacitance of supercapacitors.

Similar to acid electrolyte, alkaline electrolyte (KOH) could provide ion intercalation, without the reaction of surface functional groups, as shown in Eq. 3, and Fig. 4c shows its CV curves [74, 75]. Li$^+$, as the metal cation with minimum radius, is a frequently used neutral electrolyte ion,

such as Li_2SO_4 aqueous solution. In the cycling process, the redox reaction occurs with the reversible intercalation/deintercalation of Li$^+$. By comparison, the usage of neutral water electrolytes could improve the safety of supercapacitors. However, the oxidation of $Ti_3C_2T_x$ occurs when the potential of $Ti_3C_2T_x$ is high in aqueous electrolyte (for example, anodic oxidation when potential is over 0.6 V) [76]. As a result, it limits the expansion of voltage window of aqueous electrolyte and the energy density [77].

4.2.1.2 Ionic Liquid The application of ionic liquid electrolyte helps $Ti_3C_2T_x$ to solve this problem. Ionic liquid, a kind of molten salt, consists of organic cations and organic or inorganic anions, which keeps its liquid state at or near room temperature [78]. Jackel et al. studied the volume change of $Ti_3C_2T_x$ in ionic liquids by means of electrochemical tracing method [79]. The results show that the volume expansion of $Ti_3C_2T_x$ in ionic liquids is irreversible due to the spontaneous ion intercalation when the electrodes contact the electrolytes of ionic liquids. Volume expands at negative potential during electrochemical cycling because of the negative charge on the surface of

$Ti_3C_2T_x$, and the intercalation of cations is enhanced to maintain electrostatic equilibrium. Ion delamination and volume shrinkage of electrostatic adsorption occur at positive potential, and the permeation of solvents also has a certain effect on volume change.

In addition, the humidity of the environment causes water molecules to replace the ions on the surface of $Ti_3C_2T_x$ to increase the fluidity of the ionic liquid, so the use of this electrolyte requires humidity control [80]. The non-aqueous electrolyte solution often has a problem of poor conductivity due to large ion size, which affects the intercalation effect.

4.2.1.3 Organic Electrolyte Gogotsi et al. [81] used the lithium ion intercalation behavior of lithium hexafluorophosphate in various solvents to study the effect of electrolyte solvent on the capacitance performance. Experiments showed that the desolvation of Li intercalation is beneficial to extend the voltage window to 2.4 V and improve the capacitance performance of $Ti_3C_2T_x$. If organic solvent intercalates with Li ions, the intercalation efficiency of Li ions is reduced (Fig. 4d) [81]. At the same time, the ion conductivity of the solvent also affects the permeation of ions. Oxygen in DMSO solvent, which cannot be desolvated interacts with Li ion, keeping the hydrophobic methyl away from the surface of $Ti_3C_2T_x$. Li ion intercalation weakens the electrostatic interaction between layers.

4.2.2 The Influence of Morphology

In light of the changes in the charge and discharge process of $Ti_3C_2T_x$ in various electrolytes, the structure and morphology of $Ti_3C_2T_x$ also affect the capacitance performance. Sugahara et al. [68] used the 2D material $Ti_2C_2T_2$ to study the influence of the confinement effect on the capacitance performance and proved that the dipole polarization of the interlaminar bound water and the negative dielectric constant of the water molecule increase the specific capacitance of the material.

In addition, the lateral dimension also affects the specific capacitance of $Ti_3C_2T_x$. Maleski et al. found when it is 1 μm, the mass ratio capacitance can reach 290 F g^{-1} (2 mV s^{-1}) and the volume specific capacitance can reach 1100 F cm^{-3} [82]. When the flake size is 1.47 μm, its capacitance drops to 260 F g^{-1} [82]. This is because that smaller nanosheets have more ion diffusion paths and better ionic conductivity, and

larger nanosheets have smaller interface contact resistance and better electron conductivity.

By adjusting the time and power of ultrasonic exfoliating, the size of $Ti_3C_2T_x$ nanosheets can be controlled. The longer the ultrasonic time and the higher the power, the smaller the size of $Ti_3C_2T_x$ nanosheets. It is beneficial to increase ion diffusion sites and tighten the structure. However, the resulting material defects and increased interfacial impedance caused by ultrasonic treatment reduce the conductivity of $Ti_3C_2T_x$ [76, 83]. Anyway, while the smaller size of nanosheets introduces more ion diffusion sites, it also leads to larger interfacial contact resistance and more defects, which are detrimental to the conductivity of $Ti_3C_2T_x$. Therefore, the small size effects or the influence of ultrasonic treatment should be viewed rationally to find the balance.

4.2.3 Other Influence

As for the effect of the surface functional group, in addition to the above-mentioned participation in the pseudocapacitance reaction, the decrease in –F is good for increasing the specific capacitance, because the chemical instability of the –F functional group hinders the transfer of electrolyte ions and reduces the specific gravity of Ti ion. Moreover, the introduction of water molecules between layers results in a larger interlayer spacing, which facilitates the contact of the aqueous cations with the electrochemical active sites on the surface. Hu et al. used density functional theory (DFT) calculations to demonstrate that if the surface of $Ti_3C_2T_x$ has only –O functional group, its theoretical specific capacitance can be as high as 1190 F g^{-1} [84]. However, the presence of –F reduces the content of –O, which is the electroactive surface accessible by hydronium ions, thus hindering the transfer of electrolyte ions. If the content of –O drops to 14% of ideal value, its specific capacitance drops to 167 F g^{-1}. The increase in –O content is beneficial to the capacitance of $Ti_3C_2T_x$ tending to theoretical value. There are already methods to decline –F for Ti_2CT_x, such as annealing [85], and we believe the same strategies can be applied to $Ti_3C_2T_x$.

As shown above, many factors affect the capacitance property of $Ti_3C_2T_x$ nanosheets. There are some wrap-up problems in the usage of $Ti_3C_2T_x$ electrode materials. The first one is that the residual impure phase of the precursor phase

may lower the material quality of the prepared $Ti_3C_2T_x$, resulting in a decrease in its capacitance performance; the second one is that the precursor phase contains TiC because of excessive carbon or too little titanium due to the improper powder proportion in the sintering process; the third one is the formation of endogenous growth of alpha-alumina in the sintering process of Ti_3AlC_2 due to higher oxygen concentration during preparation. Since hydrofluoric acid etching does not affect these two impurities, the specific surface area of $Ti_3C_2T_x$ will be reduced. Since aluminum has a strong adsorption capacity for oxygen, oxygen must be strictly isolated during the preparation of Ti_3AlC_2 to avoid these two impurities [86]. The use of a conductive agent such as acetylene black during the test can suppress the orientation of the two-dimensional Ti_3C_2, provide a channel for the transfer of ions, and reduce the electrical resistance of the material as a conductive agent [86].

5 Enhancing Capacitance

From the above description, we can see that the mixed charge storage mechanism of $Ti_3C_2T_x$ determines that it is a candidate for excellent electrode materials. However, there are still some obstacles, such as stacking, oxidation, and re-crushing [87]. Its layered structure prepared by the etching method is loose, and the surface is rich in surface terminations. These negatively charged surface functional groups form a stable force—van der Waals force, which leads to stacking problems. When $Ti_3C_2T_x$ is in contact with water and air, the most oxidized part is the edge of the nanosheet. The –F functional group is gradually replaced by –O. The oxidation products (TiO_2) could significantly reduce the conductivity of $Ti_3C_2T_x$ and reduce electrolyte ion accessible sites. The increase in temperature also intensifies the tendency of Ti atoms to be oxidized. Since the etching reaction makes the surface of the material loose, the intercalation and deintercalation of the cation during charging and discharging may cause the deformation of the material or even collapse of the structure. At last, it affects the structural stability of the material, showing low rate capability. At present, many efforts have been made to solve these problems. In the following section, we discuss the measure of improving the capacitor property of $Ti_3C_2T_x$, including structure modulation method and composite reinforcement method.

5.1 Structure Modulation Method

Surface modification and film formation of $Ti_3C_2T_x$ are methods commonly used to boost the specific capacitance of $Ti_3C_2T_x$. Currently, $Ti_3C_2T_x$ aerogel also gains wide attention. In the following, these three types of strategies to increase specific capacitance of $Ti_3C_2T_x$ are discussed in detail.

5.1.1 Surface Modification

The –F functional group on the surface of $Ti_3C_2T_x$ inhibits it to obtain the desired specific capacitance. Since the Ti–F bond has lower strength at higher pH, KOH is used to alkalize $Ti_3C_2T_x$, using –OH to replace –F. According to the study of the thermal stability of $Ti_3C_2T_x$, it can be seen the surface hydroxyl group can be removed by annealing treatment, and finally, the specific gravity of the –O functional group of $Ti_3C_2T_x$ is obtained, which owns more electrochemical active sites. In addition, the annealing treatment also enhances the structural order of the material, which is advantageous for increasing the conductivity. Li et al. optimized $Ti_3C_2T_x$ through KOH alkalization and heat treatment to obtain better gravimetric capacitance of 517 F g^{-1} (1 A g^{-1}) which is about 211% of original $Ti_3C_2T_x$ [88]. Coincidentally, Zhang et al. modified $Ti_3C_2T_x$ film using the same strategy achieving high specific capacitance of 496 F g^{-1} (2 mV s^{-1}) in the H_2SO_4 electrolyte [89].

5.1.2 Film Formation

Membrane electrodes, as a common electrode, have been studied extensively in $Ti_3C_2T_x$ due to their better structural stability than powder materials. Spin coating, vacuum filtration, rolling, etc., are used to prepare thin film electrodes [90]. Some researchers deposit the fewer layers of $Ti_3C_2T_x$ organic colloid on the foamed nickel by electrophoretic deposition [91]. This method reduces the aggregation of $Ti_3C_2T_x$, increases the accessibility of the electrolyte ions, and improves the conductivity of the material. Ultimately, the specific capacitance of 140 F g^{-1} was obtained in the KOH electrolyte. Electrophoretic deposition is beneficial to the uniform penetration of $Ti_3C_2T_x$ into the three-dimensional porous structure of foamed nickel. However, if an

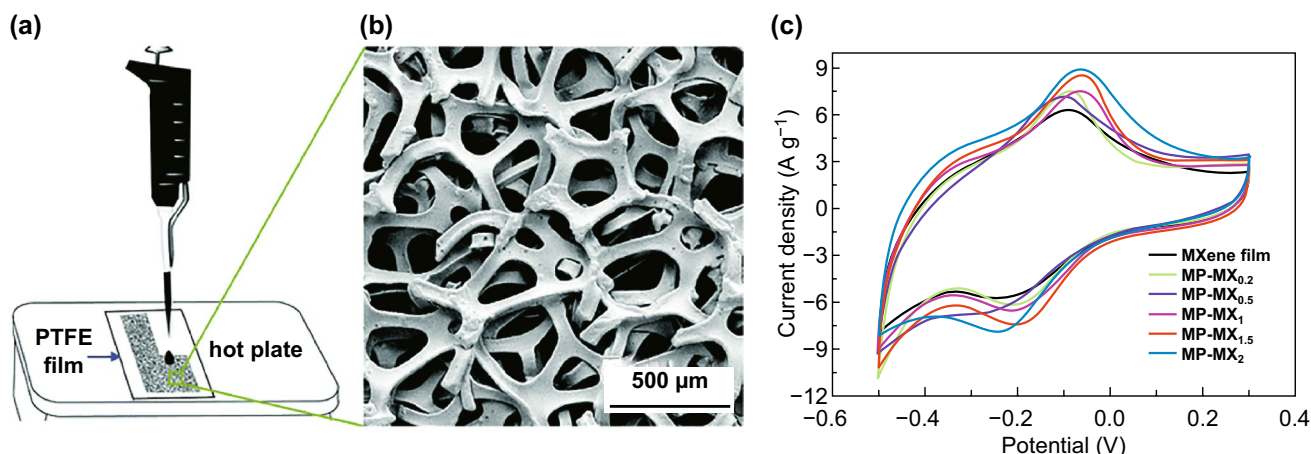**Fig. 5** $Ti_3C_2T_x$ film. **a** Schematic of the preparation of the nanoporous $Ti_3C_2T_x$ films. **b** SEM image of nickel foam [92]. **c** CV curves of $Ti_3C_2T_x$ film and modified nanoporous films at a scan rate of 10 mV s^{-1}. MP-MX$_x$ means the nanoporous $Ti_3C_2T_x$ film is obtained, where x is the mass ratio of Fe(OH)$_3$ hybrid [94]. Reproduced with permission from Refs. [92, 94]

aqueous solution is used, it will cause oxidation of $Ti_3C_2T_x$, which can be effectively avoided by using organic solvent. Hu et al. dripped the suspension on the foamed nickel and heated it at 50 °C to form a $Ti_3C_2T_x$ film, covering the foamed nickel skeleton, as shown in Fig. 5a, b [92]. This film synthesis method is called the dropping-mild baking method (DMB). The DMB method can be applied for the preparation of film-like materials with complex substrate shapes and controllable thickness. By controlling the amount of active materials in the suspension, the thickness of the film can be adjusted. When the mass loading of the film is lower, the capacitance of $Ti_3C_2T_x$ film is better, which means this method is not suitable for constructing thick electrode. The better capacitance contributes to the low impedance of ion percolation and structural stability in an acidic solution. At the same time, the structural stability can be proved by the capacitance of the film which did not have significant attenuation after 10,000 cycles [92]. The quasi-core–shell structure is formed on the foamed nickel skeleton by the negatively charged $Ti_3C_2T_x$ and the positively charged polyethyleneimine layer-by-layer electrostatic self-assembly technique, which has a larger effective contact area and fast conductive path compared with the conventional deposition method [93].

The foamed nickel skeleton forms a conductive channel to prevent re-crushing of Ti_3C_2, and wrinkles appear on the surface of the covered Ti_3C_2. Large number of mesopores provide more active sites while inhibiting the self-stacking of Ti_3C_2. However, the presence of metal collector catalyzes the decomposition of water, which decreases the voltage window of the $Ti_3C_2T_x$ material and causes an increase in electrode weight and manufacturing cost. All these limit the mass loading of active material. The appearance of porous foam-like membrane electrode can effectively solve this problem. After mixing with hydrazine hydrate, it is found that $Ti_3C_2T_x$ formed connected porous materials under high temperature and high pressure. And the reduced atmosphere formed by hydrazine hydrate significantly prevents $Ti_3C_2T_x$ oxidation and inhibits the $Ti_3C_2T_x$ stacking. Shortening the ion diffusion path is beneficial to the intercalation–deintercalation of electrolyte ions. Shi et al. [44] called the connected structure $Ti_3C_2T_x$-foam electrode which has specific capacitance of 122.7 F g^{-1} (5 mV s^{-1}) in 1 M KOH electrolyte. However, during the heat treatment, the intercalation water will have a deintercalation layer to reduce the interlayer spacing, and the decrease in the hydrophilic group content will affect the hydrophilicity of $Ti_3C_2T_x$ and reduce the ion permeation of the aqueous electrolyte. To maintain the density of the membrane electrode, nanopores are formed on the surface of the $Ti_3C_2T_x$ membrane by inserting and removing Fe(OH)$_3$ nanoparticles, thereby increasing the transport efficiency of ions [94]. Since Fe(OH)$_3$ nanoparticles are positively charged, they can be easily bonded to $Ti_3C_2T_x$, and the –F and –OH functional groups are removed by heat treatment to increase the specific gravity of Ti and the density of the film. The porous nanofilm formed by this method exhibits a wrinkle shape, suppresses the stacking of $Ti_3C_2T_x$, improves the connectivity between the nanopores,

increases the interlayer spacing, and facilitates the diffusion of ions to maintain electrochemical performance under high load conditions. Figure 5c shows the improvement between $Ti_3C_2T_x$ films and modified films [94]. Indeed, even if the mass loading reaches practical level (11.2 g cm^{-2}), it still retains an applicable capacitance (749 F cm^{-3}).

5.1.3 $Ti_3C_2T_x$ Aerogel

The preparation of $Ti_3C_2T_x$ into aerogel material can effectively increase the redox active sites to solve the problem of stacking, which can help its specific capacitance get closer to the theoretical value [67, 95]. Wan et al. utilized the overflow of ammonia gas to intercalate N atoms [40]. After that, the nanolayer wrinkles formed nanopores to suppress the stacking of nanolayers (Fig. 6a). The strong bondings on the surface such as N–Ti and O–Ti ensure a larger size for the nanolayer to enhance the stability of the structure, while

increasing the mass loading of the electrode and decreasing the specific capacitance value. The use of freeze wet gel instead of solvent produces large number of mesopores and connected structures to increase the specific surface area [96]. The extrusion effect of ethylenediamine (EDA) is used to assist the formation of Ti_3C_2 aerogel to form –NH and –NH$_2$ functional groups, and the cross section is as shown in Fig. 6b [96]. The substitution of the oxygen-containing functional group facilitates the formation of the nitrogen-containing functional group doping and the gel porous structure, but the EDA belongs to the fatty material, which muffles the redox reaction and reduces the cycle stability (Fig. 6c). After $Ti_3C_2T_x$ formed an aerogel film by vacuum-assisted filtration, the $Ti_3C_2T_x$ ion gel was prepared by immersion in an ionic liquid and vacuum drying, and large number of wrinkles appeared on the surface to increase the contact sites of the cation [97]. Due to the wide variety of ionic liquids, gel films prepared by this method have great application prospects.
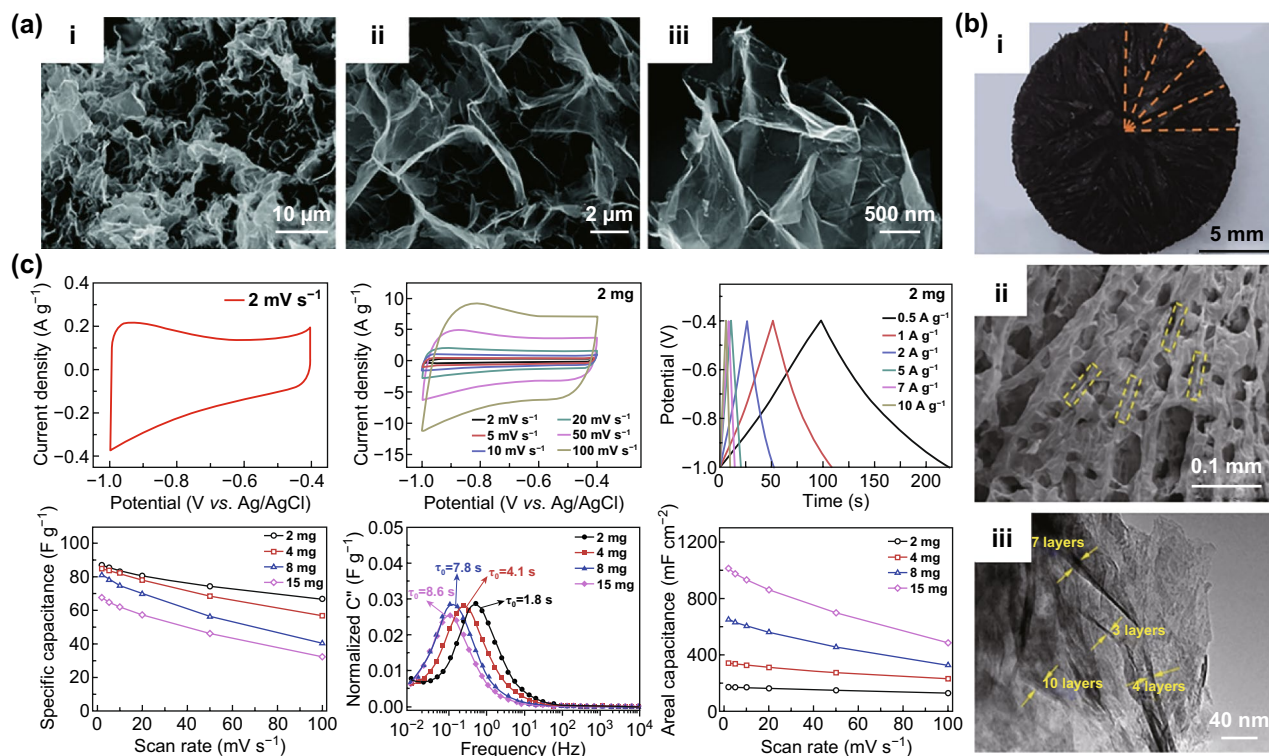

Fig. 6 $Ti_3C_2T_x$ aerogel. **a** SEM image of the $Ti_3C_2T_x$ aerogel with different magnifications [40]. **b** Cross-sectional view of Ti_3C_2 aerogel, SEM image of Ti_3C_2 aerogel, and TEM of void walls. **c** CV and GCD curves of Ti_3C_2 aerogel, specific capacitance with different mass loadings, progression of the imaginary (C″) parts of the stack capacitance of Ti_3C_2 aerogel and areal capacitance with different mass loadings [96]. Reproduced with permission from Refs. [40, 96]

5.2 Composite Method

5.2.1 Conductive Polymers (CPs)

To date, large number of researches have used electrostatic self-assembly or hydrogen bonding to combine CPs with $Ti_3C_2T_x$ to form a layered alternating sandwich structure [16, 98, 99]. The single-layer hydrated intercalation changes the content of functional groups on the surface of $Ti_3C_2T_x$, reducing –F, –OH, and interlayer water [100]. Since the pillaring effect increases the interlayer spacing of $Ti_3C_2T_x$, the bulk density of hydrazine hydrate is low and therefore does not hinder the active sites contacted with electrolyte ions. However, the intercalation of hydrazine hydrate is reversible and easily destroyed, so the structural stability is reduced after the introduction of hydrazine hydrate. PPy is one of the most common conductive polymers. The functional groups on the surface of NH and $Ti_3C_2T_x$ on the pyrrole ring form an alternating layered structure through hydrogen bonding, which is beneficial to the directional growth of PPy. PPy intercalation increases the interlayer space of $Ti_3C_2T_x$ (Fig. 7a), while this ordered structure maintains the high conductivity of $Ti_3C_2T_x$, providing a path for electrolyte ion penetration [99]. Gogotsi et al. proposed a method for the polymerization of pyrrole using acidity, avoiding the damage
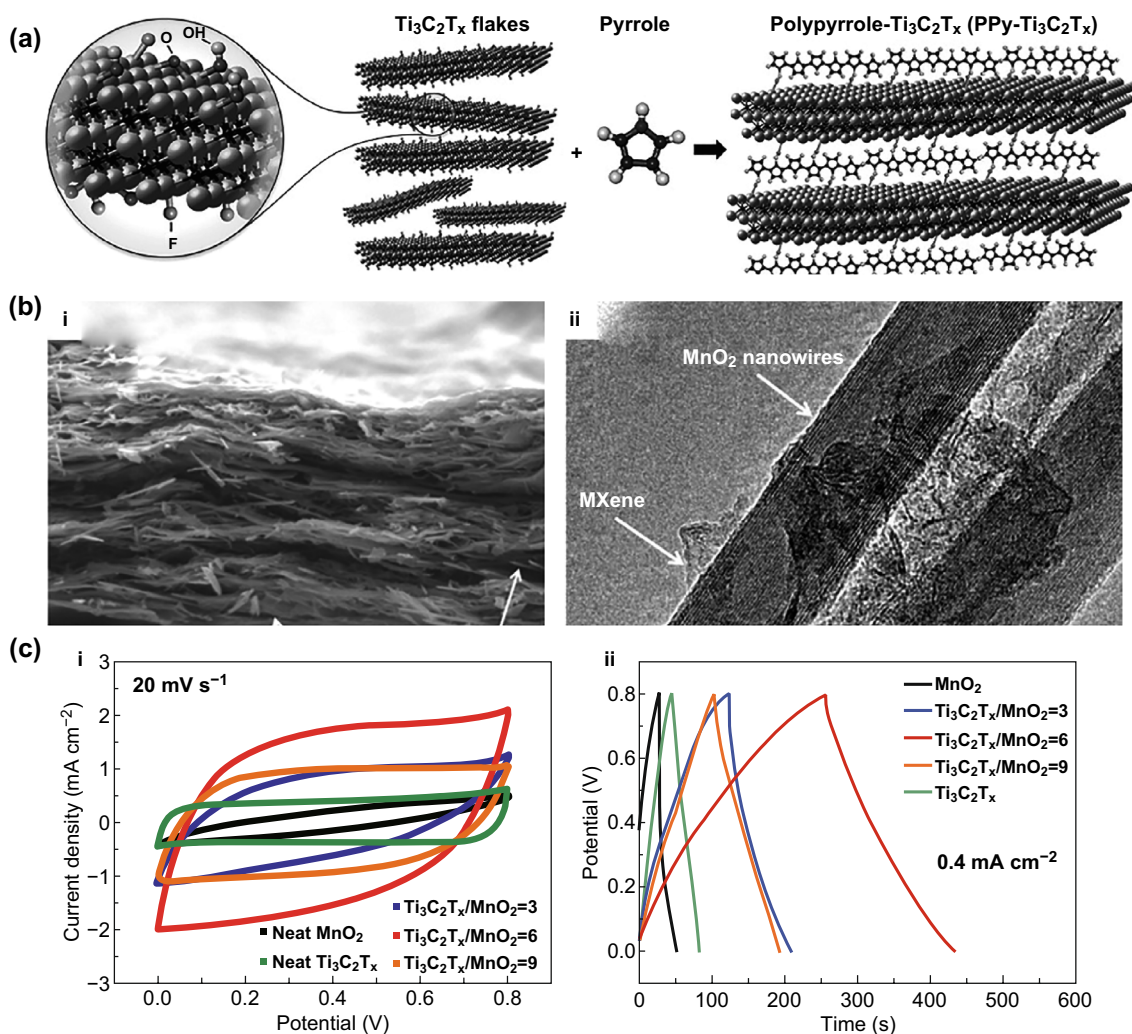
Fig. 7 $Ti_3C_2T_x$ composited with PPy and MnO_2. **a** Schematic illustration of pyrrole polymerization using $Ti_3C_2T_x$. The surface groups on the latter contribute to the polymerization process [99]. **b** Cross-sectional SEM image, and TEM image of $Ti_3C_2T_x/MnO_2$ nanowires. **c** CV and GCD curves for different samples about $Ti_3C_2T_x/MnO_2$ nanowires [104]. Reproduced with permission from Refs. [99, 104]

of oxidizing agents. But the introduction of PPy causes a slight decrease in the density of the material, and the presence of undoped PPy causes internal impedance to increase as its content increases. Wu et al. proposed low-temperature chemical oxidative polymerization forming well-arranged and uniformly distributed PPy nanoparticles [101]. It is deposited on the $Ti_3C_2T_x$ nanosheet by hydrogen bonding and electrostatic interaction (N on the PPy and the –F on the $Ti_3C_2T_x$ form electrostatic force), forming a synergistic effect. $Ti_3C_2T_x$ weakens the aggregation of PPy particles and improves the structural stability. At the same time, the intercalation of PPy expands the interlayer spacing of $Ti_3C_2T_x$ and parallels lamellar structure, shortening the diffusion path of electrolyte ions. In addition to forming a sandwich structure, the three-dimensional conductive network also has a good application prospect. One-dimensional PPy nanowires and $Ti_3C_2T_x$ nanoparticles form a three-dimensional porous structure on a foamed nickel substrate, inhibiting the aggregation between $Ti_3C_2T_x$, exposing more amorphous carbon, enhancing charge transfer rate, and introducing PPy monomer intercalation or polymerization to form an open structure around MXene, which spreads the interlayer spacing and crystallinity of $Ti_3C_2T_x$ [102].

Most methods of increasing specific capacitance are based on the premise of sacrificing density. The drawback of this strategy is to reduce the volumetric capacitance and energy density of the material. The oxidation of aniline with –O and –OH on the surface of $Ti_3C_2T_x$, the hydrophilicity of the product, causes the composite to self-polymerize, and the polyaniline (PANI) is electrochemically deposited onto the surface of $Ti_3C_2T_x$ of the composite material which causes wrinkle on the surface [43, 103]. PANI increases the layer spacing of $Ti_3C_2T_x$ to accelerate the entry of ions into the electrode material, increases the contact point of the electrolyte ions with the redox active site, and improves the conductivity of the material. In addition, the –OH and –F are reduced, and N atoms appear on the surface of the $Ti_3C_2T_x$/PANI composite film. Due to the high conductivity and ionic conductivity of the film, good specific capacitance of 371 F g^{-1} at scan rates of 2 mV s^{-1} and great capacitance retention after 10,000 cycles can be obtained even with thick electrodes (up to 45 microns) [103]. This has further broadened the use of $Ti_3C_2T_x$ in portable or self-powered devices.

5.2.2 Transition Metal Oxides (TMOs)

TMOs have the characteristics of low cost, high theoretical specific capacitance, environmental friendliness, and stable electronic transportation. The combination of $Ti_3C_2T_x$ and TMOs can effectively improve its poor conductivity. Zhou et al. [104] mixed the one-dimensional MnO_2 and $Ti_3C_2T_x$ into an ink-like material, forming a wrinkled silk-like film by solution processing, and the surface of both MnO_2 and $Ti_3C_2T_x$ was negatively charged and electrostatically repelled to form a uniform colloid (Fig. 7b, c). The composite structure produces a significant synergistic effect. The insertion of MnO_2 nanowires into the $Ti_3C_2T_x$ film increases the specific surface area. At the same time, the hybrid structure of the one-dimensional material and the two-dimensional material significantly increases the interlayer spacing and facilitates ion transport. The MnO_2 nanowires are interconnected by $Ti_3C_2T_x$ to increase the conduction speed of electrons.

The positively charged MnO_2 nanosheet and the negatively charged $Ti_3C_2T_x$ form a composite film by electrostatic self-assembly, and the electrostatic attraction makes a close relationship between the two materials and enhances the interface electron conduction capability [98]. The self-assembled structure inhibits the phenomenon of $Ti_3C_2T_x$ stacking, which is beneficial to the diffusion of ions. MnO_2 immobilized on the nanosheet promotes the uniform distribution of the ions on the surface of the electrode, improves the structural stability of the electrode, and prevents re-crushing. MnO_2 is intercalated into $Ti_3C_2T_x$ by liquid deposition and heat treatment. $Ti_3C_2T_x$ maintains its layered structure, and MnO_2 nanoparticles inhibit the stacking of the sheets [106]. The layer spacing of the material is larger than the diameter of the electrolyte cations, thereby increasing the ion intercalation. The area of the layer increases the channel for diffusion of electrolyte ions. MnO_2 forms a layered porous structure on the surface of Ti_3C_2, and the uniform distribution of MnO_2 on the surface increases the effective surface area.

In addition to MnO_2, there are many other transition metal oxide materials combined with $Ti_3C_2T_x$ to enhance its capacitance performance, like NiO [107], MoO_3 [108], WO_3 [39], Fe_2O_3 [109], TiO_2, and so on [110, 111]. Furthermore, Wang et al. [112] reported a $Ti_3C_2T_x$ composited with TMO containing two transition metal elements. According to this report, nickel and molybdenum are attached to the surface

of $Ti_3C_2T_x$ to form a flower-like connected nanostructure by using the hydrothermal method and intercalation [112]. This porous structure basically has no stacking problem commonly found in 2D materials and significantly increases the specific surface area of the material and accelerates the electrolyte. The specific area of flower-like structure is from 24.15 m^2 g^{-1} ($Ti_3C_2T_x$) to 152.3 m^2 g^{-1} [112]. During the conduction of ions, the thickness of the sheet is reduced and the pitch becomes larger to expose more electrochemically active sites. Hydrophilic $Ti_3C_2T_x$ facilitates the wettability of the electrode and shortens the path of electrolyte ion diffusion. The $Ti_3C_2T_x$/$NiMoO_4$ heterojunction prepared with this method has a specific capacitance of up to 1364 F g^{-1} in the 3 M KOH electrolyte [112]. The research ideas of

these methods are to increase the specific capacitance by the synergistic effect and TMO pseudocapacitance performance.

5.2.3 Carbon-Based Materials

There are two ways to improve the performance of MXene capacitors, i.e., forming a column effect or introducing space to increase the layer spacing [29, 113–115]. The exfoliated $Ti_3C_2T_x$ and graphene oxide (GO) mixture was vacuum-filtered into a film. After reduction heat treatment, rGO/$Ti_3C_2T_x$ hybrid film was prepared. The larger layers of rGO link the dispersed $Ti_3C_2T_x$ layers and remove some surface functional groups [116]. As a result, the conductivity of $Ti_3C_2T_x$ increases. Meanwhile, $Ti_3C_2T_x$ reduces
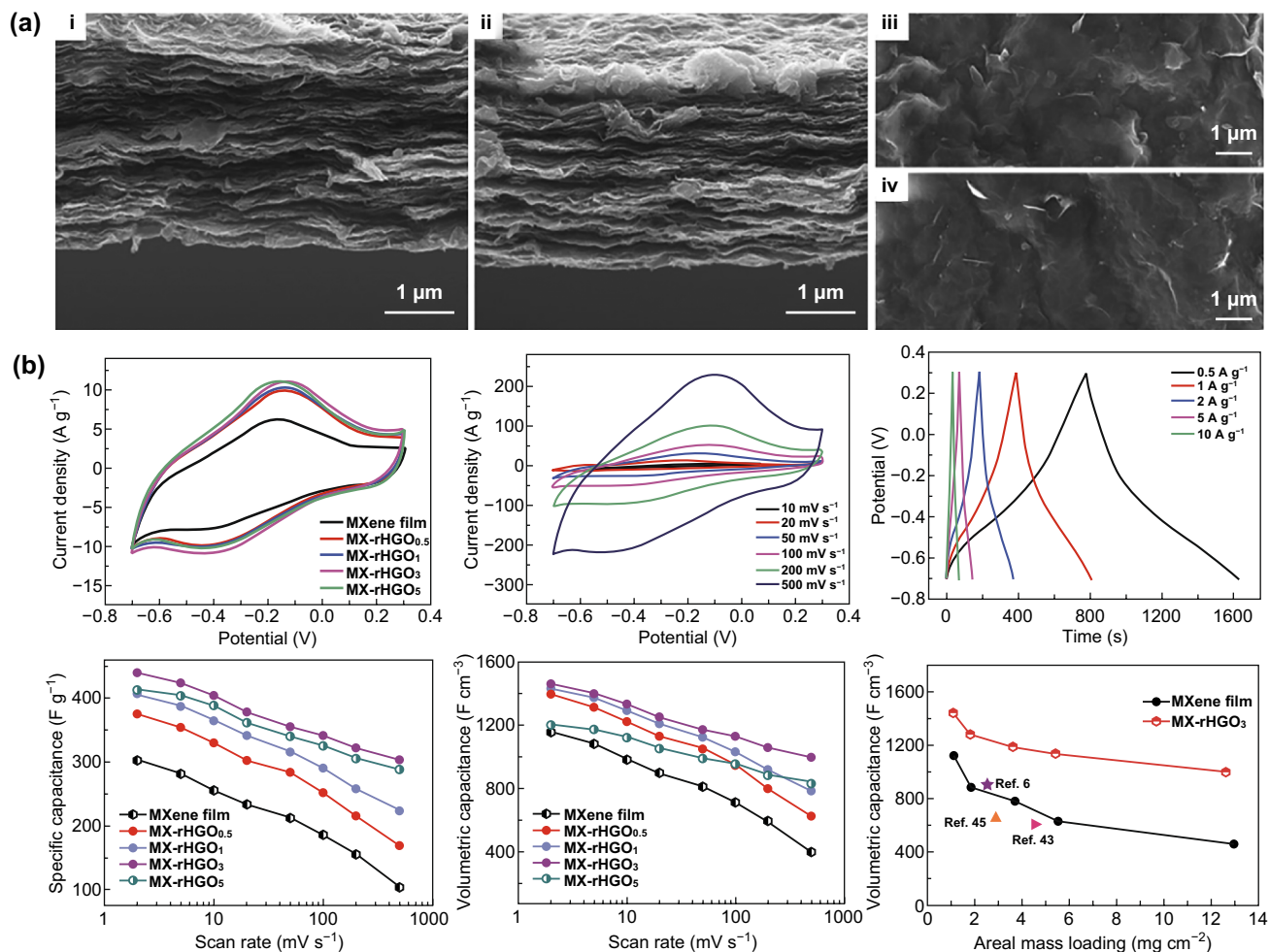
Fig. 8 $Ti_3C_2T_x$-rHGO nanoporous network. a Cross section (i, ii) and SEM images (iii, iv) of $Ti_3C_2T_x$ film (i, iii) and $Ti_3C_2T_x$-rHGO films (ii, iv). b CV and GCD curves of $Ti_3C_2T_x$ films and $Ti_3C_2T_x$-rHGO and effects of areal mass loading on the volumetric capacitance. MX-rHGO$_x$, where x is the percentage of the weight of holey graphene oxide in the mixture. Reproduced with permission from Ref. [117]

the aggregation of rGO to improve ion transport efficiency of hybrid films. Moreover, the additional polymer binder increases the accessibility of ions and reduces the internal resistance of the composite membrane. During the vacuum heating and reduction process, the oxygen surface of the GO surface is removed to cause wrinkles on the surface, which increases the specific surface area. Reduced holey graphene oxide (rGO) forms a high-connectivity nanoporous network with $Ti_3C_2T_x$, as shown in Fig. 8a [117]. Unlike other methods of forming porous composite membranes, this method retains the dense layer to maintain mechanical properties such as flexibility, and the surface area of the material is significantly increased. High volume specific capacitance of 1445 F cm^{-3} and high mass specific capacitance of 438 F g^{-1} were obtained in the 3 M H_2SO_4 electrolyte [117]. rHGO provides a large number of active sites, and this structure controls the stacking of $Ti_3C_2T_x$ to enlarge the interlayer spacing. The introduction of graphene has a slight effect on the density of $Ti_3C_2T_x$, but the volumetric

capacitance remains at a very high level, and the effect of mass loading on volumetric capacitance is not conducive to the fabrication of thick film electrodes. The CV curves of different mass ratios between $Ti_3C_2T_x$ and rGO are shown in Fig. 8b.

Fiber electrodes have become a research hot spot in the field of $Ti_3C_2T_x$, especially $Ti_3C_2T_x$ and carbon-based materials. $Ti_3C_2T_x$/carbon fiber is prepared by electrospinning $Ti_3C_2T_x$ and recarburizing PAN fiber structure. Compared with the wrapped one-dimensional electrode material, the connection between two materials is stronger, so there is no hazard of falling off of active material, helping to maintain a good conductivity and electrode stability. However, electrospinning (Fig. 9a) has the disadvantages of uneven distribution of $Ti_3C_2T_x$ and small mass loading of active material [118]. The composite of MXene and carbon tube is scrolled into a fiber-shaped spiral structure [119]. With mechanical incompatibility between carbon tube film and $Ti_3C_2T_x$ nanosheet, $Ti_3C_2T_x$ is closely related to CNTs and has high
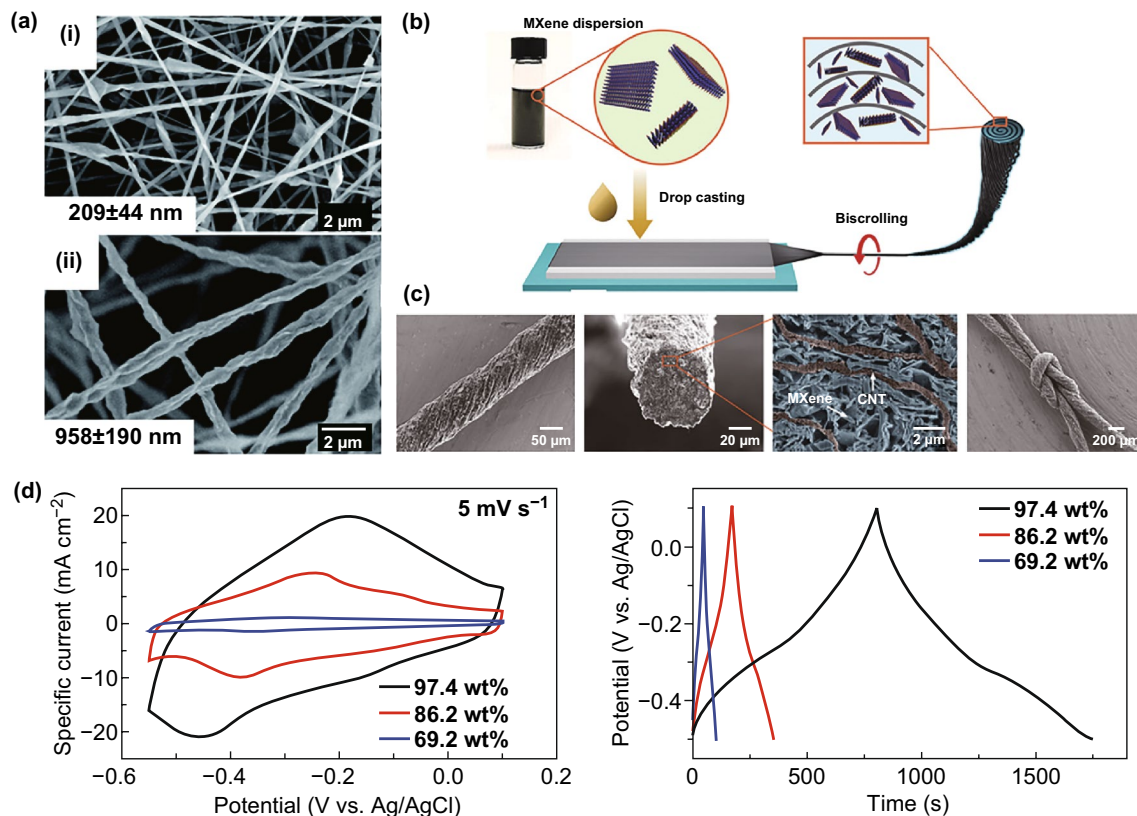
Fig. 9 One-dimensional electrode materials of supercapacitors. **a** Morphology of electrospinning $Ti_3C_2T_x$ composite [118]. **b** Schematic of the fabrication process of $Ti_3C_2T_x$ fiber using biscrolling method. **c** Surface and cross-sectional morphologies of biscrolling $Ti_3C_2T_x$ fiber. **d** CV curves obtained at 5 mV s^{-1} and GCD curves obtained at 2 mA cm^{-2} [120]. Reproduced with permission from Refs. [118, 120]

mechanical robustness and electron conductivity. Therefore, there is a gap between them to facilitate the rapid transport of ions, and the specific surface area is large. The loading of the active material in this method can not only reach a high level, but also cause an increase in the internal resistance of the composite fiber material. Biscrolling approach was used to prepare flexible fibrous materials, that is, $Ti_3C_2T_x$ drop-cast on the surface of carbon tubes and biscrolling into fibers, as shown in Fig. 9b. $Ti_3C_2T_x$ loading can be controlled simply by the adjusting the concentration of the suspension. The uniform distribution of $Ti_3C_2T_x$ (Fig. 9c) forms a lot of vacancies on the surface of the carbon tube to maintain the high conductivity of $Ti_3C_2T_x$ [120]. The electrolyte ions are infiltrated due to strong hydrophilicity. With the increase in mass loading, the specific capacitance of the material increases. When the $Ti_3C_2T_x$ mass loading is up to 98%, the specific capacitances can be as high as 1083 F cm^{-3} (428 F g^{-1}) in 3 M H_2SO_4 electrolyte, as shown in Fig. 9d.

5.2.4 Heteroatomic Doping

Doping on $Ti_3C_2T_x$ surface is a common surface modification method [44]. There are two methods for nitrogen atom doping [121]. One method is to directly anneal in ammonia gas. The N atom replaces the position of C in $Ti_3C_2T_x$, while the heat treatment removes –F functional group. Figure 10a shows the charge storage of hydrated electrolyte ions in N-doped $Ti_3C_2T_x$ [122]. The other method is solvothermal method doping N on $Ti_3C_2T_x$ surface. Compared with in-situ solid solution doping, solvothermal method can increase the specific capacitance of the material by adjusting the type and content of nitrogen source (Fig. 10b) [123]. The fluidity of ethanol and low boiling point assist the nitrogen source to diffuse between the layers. The N-doped $Ti_3C_2T_x$ surface wrinkles, containing rich N active sites and structural defects to form a connected pore structure which is beneficial to the diffusion of hydrogen ions. The surface of the doped
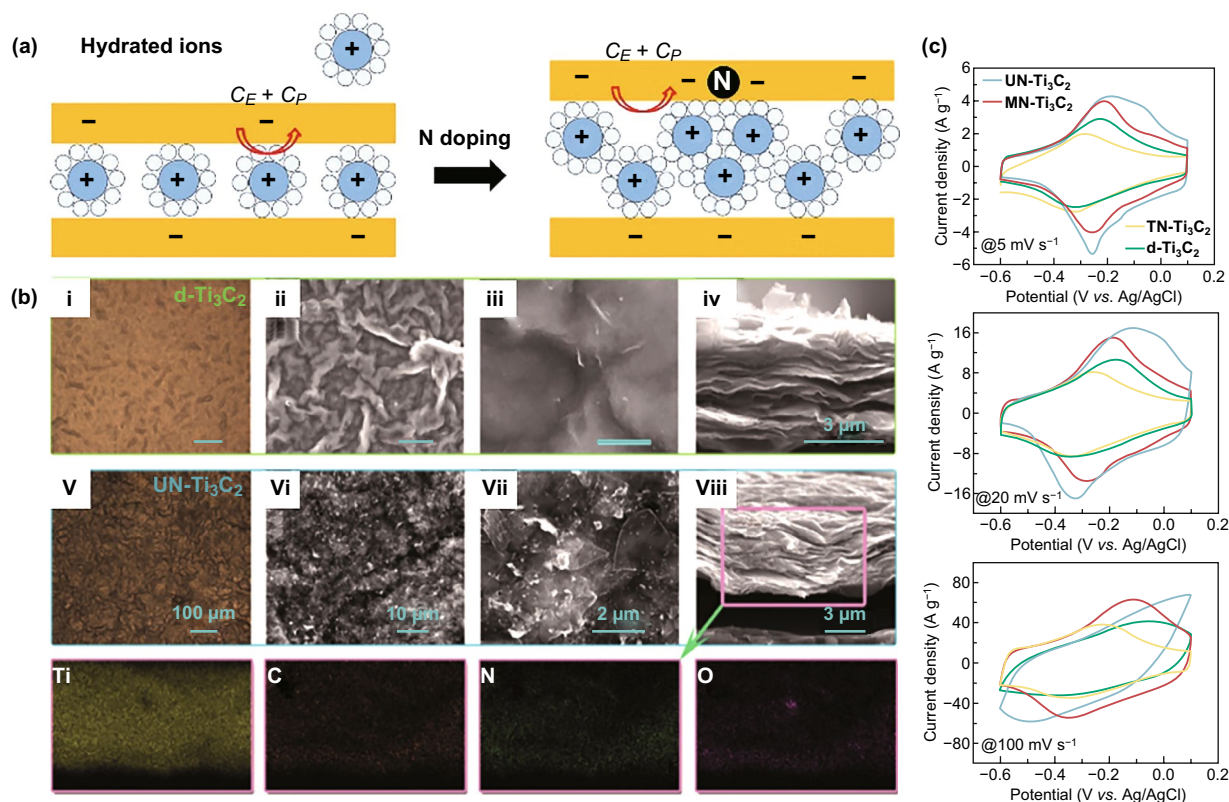
Fig. 10 N-doped $Ti_3C_2T_x$. **a** Schematic illustration of charge storage of hydrated electrolyte ions in N-doped $Ti_3C_2T_x$ [122]. **b** Plan view of optical and SEM images of Ti_3C_2 and N-doped $Ti_3C_2T_x$ using urea as the nitrogen source (UN-Ti_3C_2). **c** CV curves of the Ti_3C_2 films and N-doped Ti_3C_2 using different method, such as UN-Ti_3C_2, MN-Ti_3C_2 (nitrogen source is monoethanolamine), TN-Ti_3C_2 (solid solution method) [123]. Reproduced with permission from Refs. [122, 123]

material has mesopores and narrow slits, increasing the specific surface area. Since both the nitrogen source and $Ti_3C_2T_x$ contain oxygen functional groups, the oxidation of Ti_3C_2 is inevitable in the doping process, which affects the structural stability of the material. Nitrogen doping forms three bonding forms: Quaternary N (N-Q) contributed to N atoms replaces the position of C in the Ti_3C_2 lattice to enhance conductivity, pyrrolic N (N-5) undergoes rapid redox reaction (Fig. 10c), and N-Ti bond improves the wettability and structural stability of the electrode material [124–126]. In addition to nitrogen atom doping, N-doped carbon is also a common method [127]. The comparison of those $Ti_3C_2T_x$-based materials is shown in Table 1.

The synthesis of N-doped carbon-decorated $Ti_3C_2T_x$ complex by dopamine self-polymerization and calcination carbonization reaction effectively inhibits the $Ti_3C_2T_x$ stack from accommodating more electrolyte ions [128]. The nitrogen-doped carbon layer has a high specific surface area. $Ti_3C_2T_x$ provides higher conductivity and inhibits the agglomeration of nitrogen-doped carbon. However, due to the higher heat treatment temperature, a large amount of TiO_2 nanoparticles

are attached to the surface of the material. It is benefical to form more Ti-N bonds by increasing the N doping amount to improve the stability of the structure and increase the active suface. However, if the content is too high, the internal carbon layer cannot contact the electrolyte ions and cannot participate in the electrochemical process. The charge and discharge process will reduce the specific capacitance.

5.2.5 Other Materials

The hybridization of $Ti_3C_2T_x$ with other materials into a two-dimensional heterostructure is benefical to increase the specific surface area of the material and expose more active sites. The chemical bath deposition method was used to deposit a petal-like bismuth oxychloride (BiOCl) on the surface and between the $Ti_3C_2T_x$ nanosheets to increase the interlayer spacing of the material, which significantly increases the surface area of $Ti_3C_2T_x$ [129]. The high conductivity of BiOCl leads to rapid electron transfer and contribution of faradic reaction, and the surface of

Table 1 Comparison of capacitance performance of $Ti_3C_2T_x$-based materials, where C_s is specific capacitance

Materials	Feature	Electrolyte	C_s	Rate	References
$Ti_3C_2T_x$ aerogels	N_2 spill forming wrinkles	3 M H_2SO_4	438 F g^{-1}	10 mV s^{-1}	[40]
Freeze-dried $Ti_3C_2T_x$ aerogel	Nanoporous structure and –O replaced by NH, NH_2	1 M KOH	1012.5 mF cm^{-2}	2 mV s^{-1}	[96]
$Ti_3C_2T_x$ ion gel	Large number of wrinkles	Ion liquid	70 F g^{-1}	20 mV s^{-1}	[97]
$Ti_3C_2T_x$/PPy	Polymerization of pyrrole using acidity and no Oxidizing agents	1 M H_2SO_4	416 F g^{-1}	5 mV s^{-1}	[99]
$Ti_3C_2T_x$/PPy nanoparticles	Well-arranged, uniformly distributed PPy nanoparticles	1 M Na_2SO4	184.36 F g^{-1}	2 mV s^{-1}	[101]
$Ti_3C_2T_x$/PPy nanowires	Three-dimensional porous structure on a foamed nickel	3 M KOH	610 F g^{-1}	0.5 A g^{-1}	[102]
$Ti_3C_2T_x$/PANI	–OH and –F are reduced and N atoms appear	3 M H_2SO_4	503 F g^{-1} (1682 F cm^{-3})	2 mV s^{-1}	[103]
$Ti_3C_2T_x$/MnO_2 nanowires	Wrinkled silk-like film	PVA/LiCl	205 mF cm^{-2} (1025 F cm^{-3})	1 A cm^{-3}	[104]
$Ti_3C_2T_x$/MnO_2 nanosheet	Composite film forming by electrostatic self-assembly	1 M Na_2SO_4	340 F g^{-1}	1 A g^{-1}	[105]
$Ti_3C_2T_x$/MnO_2 nanoparticles	Layered porous structure, uniform distribution of MnO_2	6 M KOH	377 mF cm^{-2}	5 mV s^{-1}	[106]
rGO/$Ti_3C_2T_x$ hybrid film	Larger size rGO links the dispersed $Ti_3C_2T_x$ layer	6 M KOH	405 F g^{-1} (370 F cm^{-3})	1 A g^{-1}	[117]
$Ti_3C_2T_x$/CNTs	Electrospinning method	1 M H_2SO_4	205 mF cm^{-2}	50 mV s^{-1}	[118]
$Ti_3C_2T_x$/CNTs	Biscrolling approach	3 M H_2SO_4	428 F g^{-1} (1083 F cm^{-3})	2 mA cm^{-2}	[120]
$Ti_3C_2T_x$/CNTs	Scrolling into a fiber-shaped spiral structure	6 M LiCl	19.1 F cm^{-3}	1 A cm^{-3}	[119]
N-doped $Ti_3C_2T_x$	Anneal in ammonia gas directly	1 M H_2SO_4	192 F g^{-1}	1 mV s^{-1}	[122]
N-doped $Ti_3C_2T_x$	Solvothermal method (urea as nitrogen source)	3 M H_2SO_4	927 F g^{-1} (2836 F cm^{-3})	5 mV s^{-1}	[123]

the composite membrane produces a lot of mesopores to increase the accessible sites of electrolyte ions [129]. In addition, the TiO_2 particles formed by the oxidation reaction were also decomposed during the electrochemical deposition process. Ni–Co–Al layered double hydroxide (LDH) has high theoretical specific capacitance due to the two valence forms of Ni^{2+} and Co^{2+}. Zhao et al. [13] synthesized the $Ti_3C_2T_x$/Ni–Co–Al LDH heterostructures by electrostatic self-assembly, and the face-to-face contact facilitates electronic transportation.

6 Conclusions and Perspectives

MXene, as an emerging material compared with carbon materials, has aroused numerous attentions, especially in energy storage field. Among them, $Ti_3C_2T_x$ has received the most attention. In this review, we compare different etching processes and the methods for accelerating exfoliation of $Ti_3C_2T_x$. We sincerely hope that this can guide researchers to propose safer and simpler preparation process. Meanwhile, the capacitance behaviors by the two energy storage mechanisms in $Ti_3C_2T_x$ are summarized, which are cation intercalation leading to redox reaction and ion electrosorption, respectively. Influencing factors and obstacles are analyzed via electrochemical mechanism. Furthermore, we summarize the recent strategies of enhancing capacitance performance, such as film formation, synergistic effect, and heteroatom doping which lay the ground for further research to increase specific capacitance.

Based on this review, we point out the following conjectures on $Ti_3C_2T_x$ future research direction:

1. Although there are many strategies used in preparing $Ti_3C_2T_x$, the problem of low yield of $Ti_3C_2T_x$ remains unsolved and the reason is still unclear. In addition, the traditional etching processes in preparation own many security risks. Those obstacles hinder mass production and commercialization of $Ti_3C_2T_x$.
2. Thinner electrode limits the value of the material, but most improvement strategies are unsuitable for the construction of thick film. So, the electrochemical performance of thick film electrodes requires further investigation.
3. Heteroatom doping, especially N-doping, has been applied as a significant measure to improve the specific capacitance of $Ti_3C_2T_x$, and many studies have proved that wider layer spacing can be obtained after N-doping.

However, the mechanism of increasing interlayer space caused by N-doping requires further exploration.
4. The oxidation of $Ti_3C_2T_x$ is one of the most common problems. However, there are few ways to avoid it besides cryogenic storage. Non-conductive TiO_2 formed by oxidation on the surface of $Ti_3C_2T_x$ seriously affects capacitance performance, especially at the high voltages. Therefore, it is urgent to propose new feasible strategies to prevent the oxidation of $Ti_3C_2T_x$.
5. Currently, $Ti_3C_2T_x$ is mostly used as a negative electrode material for energy storage components, and its application as a positive electrode material needs to be further broadened.
6. Specific capacitance of $Ti_3C_2T_x$ is still far from ideal value, so there is still much room for improvement in the regulation of surface functional groups.

References

1. D. Larcher, J.M. Tarascon, Towards greener and more sustainable batteries for electrical energy storage. Nat. Chem. **7**, 19–29 (2015). https://doi.org/10.1038/NCHEM.2085
2. Z. Song, H. Zhou, Towards sustainable and versatile energy storage devices: an overview of organic electrode materials. Energy Environ. Sci. **6**, 2280–2301 (2013). https://doi.org/10.1039/c3ee40709h
3. N.M. Caffrey, Effect of mixed surface terminations on the structural and electrochemical properties of two-dimensional $Ti_3C_2T_2$ and V_2CT_2 MXenes multilayers. Nanoscale **10**, 13520–13530 (2018). https://doi.org/10.1039/c8nr03221a

4. H. Hu, Z. Bai, B. Niu, M. Wu, T. Hua, Binder-free bonding of modularized MXene thin films into thick film electrodes for on-chip micro-supercapacitors with enhanced areal performance metrics. J. Mater. Chem. A **6**, 14876–14884 (2018). https://doi.org/10.1039/C8TA04737E

5. D. Pech, M. Brunet, H. Durou, P. Huang, V. Mochalin, Y. Gogotsi, P.L. Taberna, P. Simon, Ultrahigh-power micrometre-sized supercapacitors based on onion-like carbon. Nat. Nanotechnol. **5**, 651–654 (2010). https://doi.org/10.1038/NNANO.2010.162

6. X. Zang, Y. Hou, T. Wang, R. Zhang, F. Kang, H. Zhu, Temperature-resistant and flexible supercapacitors based on 10-inch wafer-scale nanocarbon films. Sci. China-Mater. **62**, 947–954 (2019). https://doi.org/10.1007/s40843-018-9399-3

7. D. Hulicova-Jurcakova, M. Seredych, G.Q. Lu, N.K.A.C. Kodiweera, P.E. Stallworth, S. Greenbaum, T.J. Bandosz, Effect of surface phosphorus functionalities of activated carbons containing oxygen and nitrogen on electrochemical capacitance. Carbon **47**, 1576–1584 (2009). https://doi.org/10.1016/j.carbon.2009.02.006

8. G. Zhao, X. Li, M. Huang, Z. Zhen, Y. Zhong, Q. Chen, X. Zhao, Y. He, R. Hu, T. Yang, R. Zhang, C. Li, J. Kong, J.B. Xu, R.S. Ruoff, H. Zhu, The physics and chemistry of graphene-on-surfaces. Chem. Soc. Rev. **46**, 4417–4449 (2017). https://doi.org/10.1039/c7cs00256d

9. N. Cao, Y. Zhang, Study of Reduced Graphene Oxide Preparation by Hummers' Method and Related Characterization. J. Nanomater. **2015**, 1–5 (2015). https://doi.org/10.1155/2015/168125

10. P. Yan, J. Xu, C. Wu, R. Zhang, J. Jin, Structure and supercapacitive performance of hierarchical porous carbon obtained by catalyzing microporous carbide-derived carbon. Mater. Lett. **139**, 340–343 (2015). https://doi.org/10.1016/j.matlet.2014.10.063

11. S. Chen, Y. Xiang, M.K. Banks, C. Peng, W. Xu, R. Wu, Polyoxometalate-coupled MXene nanohybrid via poly (ionic liquid) linkers and its electrode for enhanced supercapacitive performance. Nanoscale **10**, 20043–20052 (2018). https://doi.org/10.1039/c8nr05760e

12. H. Li, F. Musharavati, E. Zalenezhad, X. Chen, K.N. Hui, K.S. Hui, Electrodeposited Ni Co layered double hydroxides on titanium carbide as a binder-free electrode for supercapacitors. Electrochim. Acta **261**, 178–187 (2018). https://doi.org/10.1016/j.electacta.2017.12.139

13. R. Zhao, M. Wang, D. Zhao, H. Li, C. Wang, L. Yin, Molecular-level heterostructures assembled from titanium carbide MXene and Ni–Co–Al layered double-hydroxide nanosheets for all-solid-state flexible asymmetric high-energy supercapacitors. ACS Energy Lett. **3**, 132–140 (2017). https://doi.org/10.1021/acsenergylett.7b01063

14. Y. Wang, H. Dou, J. Wang, B. Ding, Y. Xu, Z. Chang, X. Hao, Three-dimensional porous MXene/layered double hydroxide composite for high performance supercapacitors. J. Power Sources **327**, 221–228 (2016). https://doi.org/10.1016/j.jpowsour.2016.07.062

15. Y.-T. Weng, H.-A. Pan, N.-L. Wu, G.Z. Chen, Titanium carbide nanocube core induced interfacial growth of crystalline polypyrrole/polyvinyl alcohol lamellar shell for wide-temperature range supercapacitors. J. Power Sources **274**, 1118–1125 (2015). https://doi.org/10.1016/j.jpowsour.2014.10.158

16. H. Wang, L. Li, C. Zhu, S. Lin, J. Wen, Q. Jin, X. Zhang, In situ polymerized $Ti_3C_2T_x$/PDA electrode with superior areal capacitance for supercapacitors. J. Alloy. Compd. **778**, 858–865 (2019). https://doi.org/10.1016/j.jallcom.2018.11.172

17. M. Naguib, M. Kurtoglu, V. Presser, J. Lu, J. Niu et al., Two-dimensional nanocrystals produced by exfoliation of Ti_3AlC_2. Adv. Mater. **23**, 4248–4253 (2011). https://doi.org/10.1002/adma.201102306

18. M. Naguib, V.N. Mochalin, M.W. Barsoum, Y. Gogotsi, 25th anniversary article: mXenes: a new family of two-dimensional materials. Adv. Mater. **26**, 992–1005 (2014). https://doi.org/10.1002/adma.201304138

19. B. Anasori, M. Beidaghi, J. Lu, B.C. Hosler, L. Hultman, P.R.C. Kent, Y. Gogotsi, M.W. Barsoum, Two-dimensional, ordered, double transition metals carbides (MXenes). ACS Nano **9**, 9507–9516 (2015). https://doi.org/10.1021/acsnano.5b03591

20. M. Naguib, Y. Gogotsi, Synthesis of two-dimensional materials by selective extraction. Accounts Chem. Res. **48**, 128–135 (2015). https://doi.org/10.1021/ar500346b

21. Y. Sun, X. Meng, Y. Dall'Agnese, C. Dall'Agnese, S. Duan, Y. Gao, G. Chen, X. Wang, 2D MXenes as co-catalysts in photocatalysis: synthetic methods. Nano-Micro Lett. **11**, 79 (2019). https://doi.org/10.1007/s40820-019-0309-6

22. M. Naguib, J. Halim, J. Lu, K.M. Cook, L. Hultman, Y. Gogotsi, M.W. Barsoum, New two-dimensional niobium and vanadium carbides as promising materials for Li-ion batteries. J. Am. Chem. Soc. **135**, 15966–15969 (2013). https://doi.org/10.1021/ja405735d

23. M. Naguib, O. Mashtalir, J. Carle, V. Presser, J. Lu, L. Hultman, Y. Gogotsi, M.W. Barsoum, Two-dimensional transition metal carbides. ACS Nano **6**, 1322–1331 (2012). https://doi.org/10.1021/nn204153h

24. H.-W. Wang, M. Naguib, K. Page, D.J. Wesolowski, Y. Gogotsi, Resolving the structure of $Ti_3C_2T_x$ MXenes through multilevel structural modeling of the atomic pair distribution function. Chem. Mat. **28**, 349–359 (2015). https://doi.org/10.1021/acs.chemmater.5b04250

25. E. Kayali, A. VahidMohammadi, J. Orangi, M. Beidaghi, Controlling the dimensions of 2D MXenes for ultrahigh-rate pseudocapacitive energy storage. ACS Appl. Mater. Interfaces **10**, 25949–25954 (2018). https://doi.org/10.1021/acsami.8b07397

26. M.F. El-Kady, V. Strong, S. Dubin, R.B. Kaner, Laser scribing of high-performance and flexible graphene-based electrochemical capacitors. Science **335**, 1326–1330 (2012). https://doi.org/10.1126/science.1216744

27. L. Yu, L. Hu, B. Anasori, Y.-T. Liu, Q. Zhu, P. Zhang, Y. Gogotsi, B. Xu, MXene-bonded activated carbon as a flexible electrode for high-performance supercapacitors. ACS Energy

Lett. **3**, 1597–1603 (2018). https://doi.org/10.1021/acsenergylett.8b00718

28. R.B. Rakhi, B. Ahmed, D. Anjum, H.N. Alshareef, Direct chemical synthesis of MnO_2 nanowhiskers on transition-metal carbide surfaces for supercapacitor applications. ACS Appl. Mater. Interfaces **8**, 18806–18814 (2016). https://doi.org/10.1021/acsami.6b04481

29. J. Yan, C.E. Ren, K. Maleski, C.B. Hatter, B. Anasori, P. Urbankowski, A. Sarycheva, Y. Gogotsi, Flexible MXene/graphene films for ultrafast supercapacitors with outstanding volumetric capacitance. Adv. Funct. Mater. **27**, 1701264 (2017). https://doi.org/10.1002/adfm.201701264

30. M. Guo, C. Liu, Z. Zhang, J. Zhou, Y. Tang, S. Luo, Flexible $Ti_3C_2T_x$@Al electrodes with ultrahigh areal capacitance: in situ regulation of interlayer conductivity and spacing. Adv. Funct. Mater. **28**, 1803196 (2018). https://doi.org/10.1002/adfm.201803196

31. M. Naguib, O. Mashtalir, M.R. Lukatskaya, B. Dyatkin, C. Zhang, V. Presser, Y. Gogotsi, M.W. Barsoum, One-step synthesis of nanocrystalline transition metal oxides on thin sheets of disordered graphitic carbon by oxidation of Mxenes. Chem. Commun. **50**, 7420–7423 (2014). https://doi.org/10.1039/c4cc01646g

32. A. Lipatov, M. Alhabeb, M.R. Lukatskaya, A. Boson, Y. Gogotsi, A. Sinitskii, Effect of synthesis on quality, electronic properties and environmental stability of individual monolayer Ti_3C_2 MXene flakes. Adv. Electron. Mater. **2**, 1600255 (2016). https://doi.org/10.1002/aelm.201600255

33. H. Huang, H. Su, H. Zhang, L. Xu, X. Chu et al., Extraordinary areal and volumetric performance of flexible solid-state micro-supercapacitors based on highly conductive freestanding $Ti_3C_2T_x$ films. Adv. Electron. Mater. **4**, 1800179 (2018). https://doi.org/10.1002/aelm.201800179

34. H. Wang, J. Zhang, Y. Wu, H. Huang, Q. Jiang, Chemically functionalized two-dimensional titanium carbide MXene by in situ grafting-intercalating with diazonium ions to enhance supercapacitive performance. J. Phys. Chem. Solids **115**, 172–179 (2018). https://doi.org/10.1016/j.jpcs.2017.12.039

35. X. Jian, M. He, L. Chen, M.-M. Zhang, R. Li, L.-J. Gao, F. Fu, Z.-H. Liang, Three-dimensional carambola-like MXene/polypyrrole composite produced by one-step co-electrodeposition method for electrochemical energy storage. Electrochim. Acta **318**, 820–827 (2019). https://doi.org/10.1016/j.electacta.2019.06.045

36. L. Yu, Z. Fan, Y. Shao, Z. Tian, J. Sun, Z. Liu, Versatile N-doped MXene ink for printed electrochemical energy storage application. Adv. Energy Mater. **9**, 1901839 (2019). https://doi.org/10.1002/aenm.201901839

37. X. Wu, B. Huang, Q. Wang, Y. Wang, High energy density of two-dimensional MXene/NiCo-LDHs interstratification assembly electrode: understanding the role of interlayer ions and hydration. Chem. Eng. J. **380**, 122456 (2020). https://doi.org/10.1016/j.cej.2019.122456

38. L. Shen, X. Zhou, X. Zhang, Y. Zhang, Y. Liu, W. Wang, W. Si, X. Dong, Carbon-intercalated $Ti_3C_2T_x$ MXene for high-performance electrochemical energy storage. J. Mater.

Chem. A **6**, 23513–23520 (2018). https://doi.org/10.1039/c8ta09600g

39. S.B. Ambade, R.B. Ambade, W. Eom, S.H. Noh, S.H. Kim, T.H. Han, 2D Ti_3C_2 MXene/WO_3 hybrid architectures for high-rate supercapacitors. Adv. Mater. Interfaces **5**, 1801361 (2018). https://doi.org/10.1002/admi.201801361

40. X. Wang, Q. Fu, J. Wen, X. Ma, C. Zhu, X. Zhang, D. Qi, 3D $Ti_3C_2T_x$ aerogels with enhanced surface area for high performance supercapacitors. Nanoscale **10**, 20828–20835 (2018). https://doi.org/10.1039/c8nr06014b

41. M. Zhu, Y. Huang, Q. Deng, J. Zhou, Z. Pei et al., Highly flexible, freestanding supercapacitor electrode with enhanced performance obtained by hybridizing polypyrrole chains with MXene. Adv. Energy Mater. **6**, 1600969 (2016). https://doi.org/10.1002/aenm.201600969

42. M. Naguib, T. Saito, S. Lai, M.S. Rager, T. Aytug, M. Parans Parantham, M.-Q. Zhao, Y. Gogotsi, $Ti_3C_2T_x$ (MXene)-polyacrylamide nanocomposite films. RSC Adv. **6**, 72069–72073 (2016). https://doi.org/10.1039/c6ra10384g

43. Y. Ren, J. Zhu, L. Wang, H. Liu, Y. Liu, W. Wu, F. Wang, Synthesis of polyaniline nanoparticles deposited on two-dimensional titanium carbide for high-performance supercapacitors. Mater. Lett. **214**, 84–87 (2018). https://doi.org/10.1016/j.matlet.2017.11.060

44. L. Shi, S. Lin, L. Li, W. Wu, L. Wu, H. Gao, X. Zhang, $Ti_3C_2T_x$-foam as free-standing electrode for supercapacitor with improved electrochemical performance. Ceram. Int. **44**, 13901–13907 (2018). https://doi.org/10.1016/j.ceramint.2018.04.238

45. X.Y. Lang, B.T. Liu, X.M. Shi, Y.Q. Li, Z. Wen, Q. Jiang, Ultrahigh-power pseudocapacitors based on ordered porous heterostructures of electron-correlated oxides. Adv. Sci. **3**, 1500319 (2016). https://doi.org/10.1002/advs.201500319

46. X. Xie, M.-Q. Zhao, B. Anasori, K. Maleski, C.E. Ren et al., Porous heterostructured MXene/carbon nanotube composite paper with high volumetric capacity for sodium-based energy storage devices. Nano Energy **26**, 513–523 (2016). https://doi.org/10.1016/j.nanoen.2016.06.005

47. C. Zhou, Y. Zhang, Y. Li, J. Liu, Construction of high-capacitance 3D CoO@polypyrrole nanowire array electrode for aqueous asymmetric supercapacitor. Nano Lett. **13**, 2078–2085 (2013). https://doi.org/10.1021/nl400378j

48. A. Feng, Y. Yu, L. Mi, Y. Yu, L. Song, Comparative study on electrosorptive behavior of NH_4HF_2-etched Ti_3C_2 and HF-etched Ti_3C_2 for capacitive deionization. Ionics **25**, 727–735 (2018). https://doi.org/10.1007/s11581-018-2787-9

49. Z. Ling, C.E. Ren, M.Q. Zhao, J. Yang, J.M. Giammarco, J. Qiu, M.W. Barsoum, Y. Gogotsi, Flexible and conductive MXene films and nanocomposites with high capacitance. Proc. Natl. Acad. Sci. U.S.A. **111**, 16676–16681 (2014). https://doi.org/10.1073/pnas.1414215111

50. H. Wang, Y. Wu, X. Yuan, G. Zeng, J. Zhou, X. Wang, J.W. Chew, Clay-inspired MXene-based electrochemical devices and photo-electrocatalyst: state-of-the-art progresses and challenges. Adv. Mater. **30**, 1704561 (2018). https://doi.org/10.1002/adma.201704561

51. M.-S. Cao, Y.-Z. Cai, P. He, J.-C. Shu, W.-Q. Cao, J. Yuan, 2D MXenes: electromagnetic property for microwave absorption and electromagnetic interference shielding. Chem. Eng. J. **359**, 1265–1302 (2019). https://doi.org/10.1016/j.cej.2018.11.051

52. M. Boota, Y. Gogotsi, MXene-conducting polymer asymmetric pseudocapacitors. Adv. Energy Mater. **9**, 1901839 (2019). https://doi.org/10.1002/aenm.201802917

53. Q. Wang, Z. Zhang, Z. Zhang, X. Zhou, G. Ma, Facile synthesis of MXene/MnO$_2$ composite with high specific capacitance. J. Solid State Electrochem. **23**, 361–365 (2018). https://doi.org/10.1007/s10008-018-4143-4

54. M. Ghidiu, M.R. Lukatskaya, M.Q. Zhao, Y. Gogotsi, M.W. Barsoum, Conductive two-dimensional titanium carbide 'clay' with high volumetric capacitance. Nature **516**, 78–81 (2014). https://doi.org/10.1038/nature13970

55. M. Ghidiu, J. Halim, S. Kota, D. Bish, Y. Gogotsi, M.W. Barsoum, Ion-exchange and cation solvation reactions in Ti$_3$C$_2$ MXene. Chem. Mat. **28**, 3507–3514 (2016). https://doi.org/10.1021/acs.chemmater.6b01275

56. W. Feng, Y. Wang, S. Zeng, Y. Tan, H. Zhang, S. Peng, Ultrasonic assisted etching and delaminating of Ti$_3$C$_2$ Mxene. Ceram. Int. **44**, 7084–7087 (2018). https://doi.org/10.1016/j.ceramint.2018.01.147

57. X. Su, J. Zhang, H. Mu, J. Zhao, Z. Wang, Z. Zhao, C. Han, Z. Ye, Effects of etching temperature and ball milling on the preparation and capacitance of Ti$_3$C$_2$ MXene. J. Alloy. Compd. **752**, 32–39 (2018). https://doi.org/10.1016/j.jallcom.2018.04.152

58. Y. Tang, J. Zhu, C. Yang, F. Wang, Enhanced capacitive performance based on diverse layered structure of two-dimensional Ti$_3$C$_2$ MXene with long etching time. J. Electrochem. Soc. **163**, A1975–A1982 (2016). https://doi.org/10.1149/2.0921609jes

59. S. Yang, P. Zhang, F. Wang, A.G. Ricciardulli, M.R. Lohe, P.W.M. Blom, X. Feng, Fluoride-free synthesis of two-dimensional titanium carbide (MXene) using a binary aqueous system. Angew. Chem. Int. Ed. **57**, 15491–15495 (2018). https://doi.org/10.1002/ange.201809662

60. G. Li, L. Tan, Y. Zhang, B. Wu, L. Li, Highly efficiently delaminated single-layered MXene nanosheets with large lateral size. Langmuir **33**, 9000–9006 (2017). https://doi.org/10.1021/acs.langmuir.7b01339

61. A. Qian, J.Y. Seo, H. Shi, J.Y. Lee, C.H. Chung, Diverse surface functional groups and electrochemical behavior in dimethyl sulfoxide-delaminated Ti$_3$C$_2$T$_x$ MXene. Chem. Sus. Chem. **11**, 3719–3723 (2018). https://doi.org/10.1002/cssc.201801759

62. H. Wang, J. Zhang, Y. Wu, H. Huang, Q. Jiang, Achieving high-rate capacitance of multi-layer titanium carbide (MXene) by liquid-phase exfoliation through Li-intercalation. Electrochem. Commun. **81**, 48–51 (2017). https://doi.org/10.1016/j.elecom.2017.05.009

63. F. Han, S. Luo, L. Xie, J. Zhu, W. Wei et al., Boosting the Yield of MXene 2D Sheets via a Facile Hydrothermal-Assisted Intercalation. ACS Appl. Mater. Interfaces. **11**,

8443–8452 (2019). https://doi.org/10.1021/acsami.8b22339

64. A. Qian, S.E. Hyeon, J.Y. Seo, C.-H. Chung, Capacitance changes associated with cation-transport in free-standing flexible Ti$_3$C$_2$T$_x$ (T = O, F, OH) MXene film electrodes. Electrochim. Acta **266**, 86–93 (2018). https://doi.org/10.1016/j.electacta.2018.02.019

65. Y. Ando, Y. Gohda, S. Tsuneyuki, Ab initio molecular dynamics study of the Helmholtz layer formed on solid-liquid interfaces and its capacitance. Chem. Phys. Lett. **556**, 9–12 (2013). https://doi.org/10.1016/j.cplett.2012.11.062

66. M. Acerce, D. Voiry, M. Chhowalla, Metallic 1T phase MoS$_2$ nanosheets as supercapacitor electrode materials. Nat. Nanotechnol. **10**, 313–318 (2015). https://doi.org/10.1038/NNANO.2015.40

67. M.R. Lukatskaya, S. Kota, Z. Lin, M.-Q. Zhao, N. Shpigel et al., Ultra-high-rate pseudocapacitive energy storage in two-dimensional transition metal carbides. Nat. Energy **2**, 17105 (2017). https://doi.org/10.1038/nenergy.2017.105

68. A. Sugahara, Y. Ando, S. Kajiyama, K. Yazawa, K. Gotoh, M. Otani, M. Okubo, A. Yamada, Negative dielectric constant of water confined in nanosheets. Nat. Commun. **10**, 850 (2019). https://doi.org/10.1038/s41467-019-08789-8

69. P. Simon, Y. Gogotsi, B. Dunn, Where do batteries end and supercapacitors begin. Science **343**, 1210–1211 (2014). https://doi.org/10.1126/science.1249625

70. Q.X. Xia, N.M. Shinde, T. Zhang, J.M. Yun, A. Zhou, R.S. Mane, S. Mathur, K.H. Kim, Seawater electrolyte-mediated high volumetric MXene-based electrochemical symmetric supercapacitors. Dalton Trans. **47**, 8676–8682 (2018). https://doi.org/10.1039/C8DT01375F

71. M. Hu, Z. Li, T. Hu, S. Zhu, C. Zhang, X. Wang, High-capacitance mechanism for Ti$_3$C$_2$T$_x$ MXene by in situ electrochemical Raman spectroscopy investigation. ACS Nano **10**, 11344–11350 (2016). https://doi.org/10.1021/acsnano.6b06597

72. C. Zhan, M. Naguib, M. Lukatskaya, P.R.C. Kent, Y. Gogotsi, D.E. Jiang, Understanding the MXene pseudocapacitance. J. Phys. Chem. Lett. **9**, 1223–1228 (2018). https://doi.org/10.1021/acs.jpclett.8b00200

73. Y. Dall'Agnese, M.R. Lukatskaya, K.M. Cook, P.-L. Taberna, Y. Gogotsi, P. Simon, High capacitance of surface-modified 2D titanium carbide in acidic electrolyte. Electrochem. Commun. **48**, 118–122 (2014). https://doi.org/10.1016/j.elecom.2014.09.002

74. R. Syamsai, P. Kollu, S. Kwan Jeong, A. Nirmala Grace, Synthesis and properties of 2D-titanium carbide MXene sheets towards electrochemical energy storage applications. Ceram. Int. **43**, 13119–13126 (2017). https://doi.org/10.1016/j.ceramint.2017.07.003

75. Y. Gao, L. Wang, Z. Li, Y. Zhang, B. Xing, C. Zhang, A. Zhou, Electrochemical performance of Ti$_3$C$_2$ supercapacitors in KOH electrolyte. J. Adv. Ceram. **4**, 130–134 (2015). https://doi.org/10.1007/s40145-015-0143-3

76. Y.-Y. Peng, B. Akuzum, N. Kurra, M.-Q. Zhao, M. Alhabeb et al., All-MXene (2D titanium carbide) solid-state

microsupercapacitors for on-chip energy storage. Energy Environ. Sci. **9**, 2847–2854 (2016). https://doi.org/10.1039/c6ee01717g

77. Y. Dall'Agnese, P. Rozier, P.-L. Taberna, Y. Gogotsi, P. Simon, Capacitance of two-dimensional titanium carbide (MXene) and MXene/carbon nanotube composites in organic electrolytes. J. Power Sources **306**, 510–515 (2016). https://doi.org/10.1016/j.jpowsour.2015.12.036

78. K.R. Seddon, Ionic Liquids for Clean Technology. J. Chem. Tech. Biotechnol. **68**, 351–356 (1997). https://doi.org/10.1002/(SICI)1097-4660(199704)68:4%3c351:AID-JCTB613%3e3.0.CO;2-4

79. N. Jackel, B. Kruner, K.L. Van Aken, M. Alhabeb, B. Anasori, F. Kaasik, Y. Gogotsi, V. Presser, Electrochemical in situ tracking of volumetric changes in two-dimensional metal carbides (MXenes) in ionic liquids. ACS Appl. Mater. Interfaces **8**, 32089–32093 (2016). https://doi.org/10.1021/acsami.6b11744

80. N.C. Osti, M.W. Thompson, K.L. Van Aken, M. Alhabeb, M. Tyagi et al., Humidity exposure enhances microscopic mobility in a room-temperature ionic liquid in MXene. J. Phy. Chem. C **122**, 27561–27566 (2018). https://doi.org/10.1021/acs.jpcc.8b09677

81. X. Wang, T.S. Mathis, K. Li, Z. Lin, L. Vlcek et al., Influences from solvents on charge storage in titanium carbide Mxenes. Nat. Energy **4**, 241–248 (2019). https://doi.org/10.1038/s41560-019-0339-9

82. K. Maleski, C.E. Ren, M.Q. Zhao, B. Anasori, Y. Gogotsi, Size-dependent physical and electrochemical properties of two-dimensional MXene flakes. ACS Appl. Mater. Interfaces **10**, 24491–24498 (2018). https://doi.org/10.1021/acsami.8b04662

83. H. Wang, Y. Wu, J. Zhang, G. Li, H. Huang, X. Zhang, Q. Jiang, Enhancement of the electrical properties of MXene Ti_3C_2 nanosheets by post-treatments of alkalization and calcination. Mater. Lett. **160**, 537–540 (2015). https://doi.org/10.1016/j.matlet.2015.08.046

84. M. Hu, T. Hu, Z. Li, Y. Yang, R. Cheng, J. Yang, C. Cui, X. Wang, Surface functional groups and interlayer water determine the electrochemical capacitance of $Ti_3C_2T_x$ Mxene. ACS Nano **12**, 3578–3586 (2018). https://doi.org/10.1021/acsnano.8b00676

85. R.B. Rakhi, B. Ahmed, M.N. Hedhili, D.H. Anjum, H.N. Alshareef, Effect of postetch annealing gas composition on the structural and electrochemical properties of Ti_2CT_x MXene electrodes for supercapacitor applications. Chem. Mat. **27**, 5314–5323 (2015). https://doi.org/10.1021/acs.chemmater.5b01623

86. B. Scheibe, V. Kupka, B. Peplinska, M. Jarek, K. Tadyszak, The influence of oxygen concentration during MAX phases (Ti_3AlC_2) preparation on the alpha-Al_2O_3 microparticles content and specific surface area of multilayered MXenes ($Ti_3C_2T_x$). Materials **12**, 253 (2019). https://doi.org/10.3390/ma12030353

87. C. Zhao, Q. Wang, H. Zhang, S. Passerini, X. Qian, Two-dimensional titanium carbide/RGO composite for high-performance supercapacitors. ACS Appl. Mater. Interfaces **8**, 15661–15667 (2016). https://doi.org/10.1021/acsami.6b04767

88. J. Li, X. Yuan, C. Lin, Y. Yang, L. Xu, X. Du, J. Xie, J. Lin, J. Sun, Achieving high pseudocapacitance of 2D titanium carbide (MXene) by cation intercalation and surface modification. Adv. Energy Mater. **7**, 1602725 (2017). https://doi.org/10.1002/aenm.201602725

89. X. Zhang, Y. Liu, S. Dong, J. Yang, X. Liu, Surface modified MXene film as flexible electrode with ultrahigh volumetric capacitance. Electrochim. Acta **294**, 233–239 (2019). https://doi.org/10.1016/j.electacta.2018.10.096

90. C.J. Zhang, B. Anasori, A. Seral-Ascaso, S.H. Park, N. McEvoy et al., Transparent, flexible, and conductive 2D titanium carbide (MXene) films with high volumetric capacitance. Adv. Mater. **29**, 1702678 (2017). https://doi.org/10.1002/adma.201702678

91. S. Xu, G. Wei, J. Li, Y. Ji, N. Klyui, V. Izotov, W. Han, Binder-free $Ti_3C_2T_x$ MXene electrode film for supercapacitor produced by electrophoretic deposition method. Chem. Eng. J. **317**, 1026–1036 (2017). https://doi.org/10.1039/C8TA04737E

92. M. Hu, Z. Li, H. Zhang, T. Hu, C. Zhang, Z. Wu, X. Wang, Self-assembled $Ti_3C_2T_x$ MXene film with high gravimetric capacitance. Chem. Commun. **51**, 13531–13533 (2015). https://doi.org/10.1039/c5cc04722f

93. Y. Tian, C. Yang, W. Que, Y. He, X. Liu, Y. Luo, X. Yin, L.B. Kong, Ni foam supported quasi-core-shell structure of ultrathin Ti_3C_2 nanosheets through electrostatic layer-by-layer self-assembly as high rate-performance electrodes of supercapacitors. J. Power Sources **369**, 78–86 (2017). https://doi.org/10.1016/j.jpowsour.2017.09.085

94. Z. Fan, Y. Wang, Z. Xie, X. Xu, Y. Yuan, Z. Cheng, Y. Liu, A nanoporous MXene film enables flexible supercapacitors with high energy storage. Nanoscale **10**, 9642–9652 (2018). https://doi.org/10.1039/c8nr01550c

95. R. Liu, A. Zhang, J. Tang, J. Tian, W. Huang, J. Cai, C. Barrow, W. Yang, J. Liu, Fabrication of cobaltosic oxide nanoparticle-doped 3D MXene/graphene hybrid porous aerogels for all-solid-state supercapacitors. Chem. Eur. J. **25**, 5547–5554 (2019). https://doi.org/10.1002/chem.201806342

96. L. Li, M. Zhang, X. Zhang, Z. Zhang, New Ti_3C_2 aerogel as promising negative electrode materials for asymmetric supercapacitors. J. Power Sources **364**, 234–241 (2017). https://doi.org/10.1016/j.jpowsour.2017.08.029

97. Z. Lin, D. Barbara, P.-L. Taberna, K.L. Van Aken, B. Anasori, Y. Gogotsi, P. Simon, Capacitance of $Ti_3C_2T_x$ MXene in ionic liquid electrolyte. J. Power Sources **326**, 575–579 (2016). https://doi.org/10.1016/j.jpowsour.2016.04.035

98. J. Yan, Y. Ma, C. Zhang, X. Li, W. Liu, X. Yao, S. Yao, S. Luo, Polypyrrole-MXene coated textile-based flexible energy storage device. RSC Adv. **8**, 39742–39748 (2018). https://doi.org/10.1039/c8ra08403c

99. M. Boota, B. Anasori, C. Voigt, M.Q. Zhao, M.W. Barsoum, Y. Gogotsi, Pseudocapacitive electrodes produced by oxidant-free polymerization of pyrrole between the layers of

2D titanium carbide (MXene). Adv. Mater. **28**, 1517–1522 (2016). https://doi.org/10.1002/adma.201504705

100. O. Mashtalir, M.R. Lukatskaya, A.I. Kolesnikov, E. Raymundo-Pinero, M. Naguib, M.W. Barsoum, Y. Gogotsi, The effect of hydrazine intercalation on the structure and capacitance of 2D titanium carbide (MXene). Nanoscale **8**, 9128–9133 (2016). https://doi.org/10.1039/c6nr01462c

101. W. Wu, D. Wei, J. Zhu, D. Niu, F. Wang et al., Enhanced electrochemical performances of organ-like Ti_3C_2 MXenes/polypyrrole composites as supercapacitors electrode materials. Ceram. Int. **45**, 7328–7337 (2019). https://doi.org/10.1016/j.ceramint.2019.01.016

102. T.A. Le, N.Q. Tran, Y. Hong, H. Lee, Intertwined titanium carbide MXene within a 3D tangled polypyrrole nanowires matrix for enhanced supercapacitor performances. Chem. Eur. J. **25**, 1037–1043 (2019). https://doi.org/10.1002/chem.201804291

103. A. VahidMohammadi, J. Moncada, H. Chen, E. Kayali, J. Orangi, C.A. Carrero, M. Beidaghi, Thick and freestanding MXene/PANI pseudocapacitive electrodes with ultrahigh specific capacitance. J. Mater. Chem. A **6**, 22123–22133 (2018). https://doi.org/10.1039/c8ta05807e

104. J. Zhou, J. Yu, L. Shi, Z. Wang, H. Liu, B. Yang, C. Li, C. Zhu, J. Xu, A Conductive and highly deformable all-pseudocapacitive composite paper as supercapacitor electrode with improved areal and volumetric capacitance. Small **14**, 1803786 (2018). https://doi.org/10.1002/smll.201803786

105. S. Chen, Y. Xiang, W. Xu, C. Peng, A novel MnO_2/MXene composite prepared by electrostatic self-assembly and its use as an electrode for enhanced supercapacitive performance. Inorg. Chem. Front. **6**, 199–208 (2019). https://doi.org/10.1039/c8qi00957k

106. Y. Tang, J. Zhu, C. Yang, F. Wang, Enhanced supercapacitive performance of manganese oxides doped two-dimensional titanium carbide nanocomposite in alkaline electrolyte. J. Alloy. Compd. **685**, 194–201 (2016). https://doi.org/10.1016/j.jallcom.2016.05.221

107. K. Zhang, G. Ying, L. Liu, F. Ma, L. Su, C. Zhang, D. Wu, X. Wang, Y. Zhou, Three-dimensional porous $Ti_3C_2T_x$-NiO composite electrodes with enhanced electrochemical performance for supercapacitors. Materials **12**, 188 (2019). https://doi.org/10.3390/ma12010188

108. J. Zhu, X. Lu, L. Wang, Synthesis of a MoO_3/$Ti_3C_2T_x$ composite with enhanced capacitive performance for supercapacitors. RSC Adv. **6**, 98506–98513 (2016). https://doi.org/10.1039/c6ra15651g

109. R. Zou, H. Quan, M. Pan, S. Zhou, D. Chen, X. Luo, Self-assembled MXene($Ti_3C_2T_x$)/α-Fe_2O_3 nanocomposite as negative electrode material for supercapacitors. Electrochim. Acta **292**, 31–38 (2018). https://doi.org/10.1016/j.electacta.2018.09.149

110. J. Zhu, C. Yang, F. Wang, M. Cao, Composites of TiO_2 nanoparticles deposited on Ti_3C_2 MXene nanosheets with enhanced electrochemical performance. J. Electrochem. Soc. **163**, A785 (2016). https://doi.org/10.1149/2.0981605jes

111. W. Zheng, P. Zhang, W. Tian, Y. Wang, Y. Zhang, J. Chen, Z. Sun, Microwave-assisted synthesis of SnO_2-Ti_3C_2 nanocomposite for enhanced supercapacitive performance. Mater. Lett. **209**, 122–125 (2017). https://doi.org/10.1016/j.matlet.2017.07.131

112. Y. Wang, J. Sun, X. Qian, Y. Zhang, L. Yu, R. Niu, H. Zhao, J. Zhu, 2D/2D heterostructures of nickel molybdate and MXene with strong coupled synergistic effect towards enhanced supercapacitor performance. J. Power Sources **414**, 540–546 (2019). https://doi.org/10.1016/j.jpowsour.2019.01.036

113. Q. Fu, X. Wang, N. Zhang, J. Wen, L. Li, H. Gao, X. Zhang, Self-assembled $Ti_3C_2T_x$/SCNT composite electrode with improved electrochemical performance for supercapacitor. J. Colloid Interface Sci. **511**, 128–134 (2018). https://doi.org/10.1016/j.jcis.2017.09.104

114. L. Yang, W. Zheng, P. Zhang, J. Chen, W.B. Tian, Y.M. Zhang, Z.M. Sun, MXene/CNTs films prepared by electrophoretic deposition for supercapacitor electrodes. J. Electroanal. Chem. **830**, 1–6 (2018). https://doi.org/10.1016/j.jelechem.2018.10.024

115. M.Q. Zhao, C.E. Ren, Z. Ling, M.R. Lukatskaya, C. Zhang, K.L. Van Aken, M.W. Barsoum, Y. Gogotsi, Flexible MXene/carbon nanotube composite paper with high volumetric capacitance. Adv. Mater. **27**, 339–345 (2015). https://doi.org/10.1002/adma.201404140

116. S. Xu, G. Wei, J. Li, W. Han, Y. Gogotsi, Flexible Mxene-graphene electrodes with high volumetric capacitance for integrated co-cathode energy conversion/storage devices. J. Mater. Chem. A **5**, 17442–17451 (2017). https://doi.org/10.1039/c7ta05721k

117. Z. Fan, Y. Wang, Z. Xie, D. Wang, Y. Yuan, H. Kang, B. Su, Z. Cheng, Y. Liu, Modified MXene/holey graphene films for advanced supercapacitor electrodes with superior energy storage. Adv. Sci. **5**, 1800750 (2018). https://doi.org/10.1002/advs.201800750

118. A.S. Levitt, M. Alhabeb, C.B. Hatter, A. Sarycheva, G. Dion, Y. Gogotsi, Electrospun MXene/carbon nanofibers as supercapacitor electrodes. J. Mater. Chem. A **7**, 269–277 (2019). https://doi.org/10.1039/c8ta09810g

119. C. Yu, Y. Gong, R. Chen, M. Zhang, J. Zhou, J. An, F. Lv, S. Guo, G. Sun, A solid-state fibriform supercapacitor boosted by host-guest hybridization between the carbon nanotube Scaffold and MXene nanosheets. Small **14**, 1801203 (2018). https://doi.org/10.1002/smll.201801203

120. Z. Wang, S. Qin, S. Seyedin, J. Zhang, J. Wang et al., High-performance biscrolled MXene/carbon nanotube yarn supercapacitors. Small **14**, 1802225 (2018). https://doi.org/10.1002/smll.201802225

121. L. Yang, W. Zheng, P. Zhang, J. Chen, W. Zhang, W.B. Tian, Z.M. Sun, Freestanding nitrogen-doped d-Ti_3C_2/reduced graphene oxide hybrid films for high performance supercapacitors. Electrochim. Acta **300**, 349–356 (2019). https://doi.org/10.1016/j.electacta.2019.01.122

122. Y. Wen, T.E. Rufford, X. Chen, N. Li, M. Lyu, L. Dai, L. Wang, Nitrogen-doped $Ti_3C_2T_x$ MXene electrodes for

high-performance supercapacitors. Nano Energy **38**, 368–376 (2017). https://doi.org/10.1016/j.nanoen.2017.06.009

123. C. Yang, Y. Tang, Y. Tian, Y. Luo, M.F.U. Din, X. Yin, W. Que, Flexible nitrogen-doped 2D titanium carbides (MXene) films constructed by an ex situ solvothermal method with extraordinary volumetric capacitance. Adv. Energy Mater. **8**, 1802087 (2018). https://doi.org/10.1002/aenm.201802087

124. G. Kresse, Ab initio molecular dynamics for liquid metals. J. Non-Ctyst. Solids **192&193**, 222–229 (1993). https://doi.org/10.1103/PhysRevB.47.558

125. G. Kresse, J. Furthmüller, Efficient iterative schemes for ab initio total-energy calculations using a plane-wave basis set. Am. Phys. Soc. **54**, 11169–11186 (1996). https://doi.org/10.1103/PhysRevB.54.11169

126. F.M. Hassan, V. Chabot, J. Li, B.K. Kim, L. Ricardez-Sandoval, A. Yu, Pyrrolic-structure enriched nitrogen doped graphene for highly efficient next generation supercapacitors.

J. Mater. Chem. A **1**, 2904–2912 (2013). https://doi.org/10.1039/c2ta01064j

127. C. Zhang, L. Wang, W. Lei, Y. Wu, C. Li et al., Achieving quick charge/discharge rate of 3.0 Vs^{-1} by 2D titanium carbide (MXene) via N-doped carbon intercalation. Mater. Lett. **234**, 21–25 (2019). https://doi.org/10.1016/j.matlet.2018.08.124

128. T. Zhao, J. Zhang, Z. Du, Y. Liu, G. Zhou, J. Wang, Dopamine-derived N-doped carbon decorated titanium carbide composite for enhanced supercapacitive performance. Electrochim. Acta **254**, 308–319 (2017). https://doi.org/10.1016/j.electacta.2017.09.144

129. Q.X. Xia, N.M. Shinde, J.M. Yun, T. Zhang, R.S. Mane, S. Mathur, K.H. Kim, Bismuth oxychloride/MXene symmetric supercapacitor with high volumetric energy density. Electrochim. Acta **271**, 351–360 (2018). https://doi.org/10.1016/j.electacta.2018.03.168